CHALMERS
UNIVERSITY OF TECHNOLOGY

Recent Progress in Ab Initio Nuclear Theory for Precision Physics Searches in Muonic Atoms and Superallowed β Decays

Downloaded from: https://research.chalmers.se, 2026-10-27 23:05 UTC

Citation for the original published paper (version of record):
Li Muli, S., Gennari, M. (2026). Recent Progress in Ab Initio Nuclear Theory for Precision Physics Searches in Muonic Atoms and
Superallowed β Decays. Atoms, 14(9). http://dx.doi.org/10.3390/atoms14090074

N.B. When citing this work, cite the original published paper.

research.chalmers.se offers the possibility of retrieving research publications produced at Chalmers University of Technology. It covers all kind of research output: articles, dissertations, conference papers, reports etc. since 2004. research.chalmers.se is administrated and maintained by Chalmers Library

(article starts on next page)

atoms

MDPI

Review

Recent Progress in *Ab Initio* Nuclear Theory for Precision Physics Searches in Muonic Atoms and Superallowed β Decays

Simone Salvatore Li Muli [1,*] and Michael Gennari [2]

[1] Department of Physics, Chalmers University of Technology, 412 96 Gothenburg, Sweden
[2] Institut für Kernphysik and PRISMA^{++} Cluster of Excellence, Johannes Gutenberg-Universität Mainz, 55128 Mainz, Germany; mgennari@uni-mainz.de
* Correspondence: simone.limuli@chalmers.se

Abstract

Precision tests of the Standard Model at low energy are increasingly limited by nuclear-structure theory rather than by experiments. We review two such cases: the two-photon-exchange correction to the Lamb shift in muonic atoms, and the γW box radiative correction to superallowed β decays. Although they probe different physics, both are governed by the same generalized hadronic tensor, so that the chiral effective field theory Hamiltonians and currents, Lanczos-based response methods, and Bayesian uncertainty quantification developed for one carry over directly to the other. We summarize recent *ab initio* progress in light nuclei and its impact on nuclear charge radii, on the helium isotope-shift puzzle, and on the extraction of V_{ud} for the top-row CKM unitarity test, and state a future outlook.

Keywords: *ab initio* nuclear theory; muonic atoms; superallowed beta decay; nuclear polarizability; radiative corrections; electroweak interactions; Standard Model tests; chiral effective field theory

Check for updates

Academic Editors: Shihang Shen, Peng Yin and Baishan Hu

Received: 28 July 2026
Revised: 23 August 2026
Accepted: 26 August 2026
Published: 4 September 2026

Copyright: © 2026 by the authors. Licensee MDPI, Basel, Switzerland. This article is an open access article distributed under the terms and conditions of the Creative Commons Attribution (CC BY) license.

1. Introduction

The Standard Model (SM) of particle physics, despite its extraordinary empirical success, leaves fundamental questions unanswered. For example, the origin of neutrino masses, the nature of dark matter, and the baryon asymmetry of the universe, among others. It is, therefore, widely regarded as the low-energy limit of a more complete theory. Searches for its extensions proceed along two complementary lines. At the energy frontier, collider experiments aim to produce new particles directly. At the precision frontier, one confronts observables that can be both measured and computed with high accuracy where virtual contributions of new interactions would appear as small but systematic deviations between experiment and SM prediction [1,2]. In an effective-field-theory (EFT) description, new interactions arising at a scale, Λ, induce low-energy couplings suppressed by $(v/\Lambda)^2$, with v the electroweak vacuum expectation value, so that experiments sensitive to relative deviations at the $\mathcal{O}(10^{-3})$ to $\mathcal{O}(10^{-4})$ level probe effective scales of order 10 TeV and beyond, that is to say, at or above the direct reach of the Large Hadron Collider [1,2]. Atomic nuclei and atomic bound states, which can be prepared and measured with exceptional control, host several flagship tests of this kind [3]; this review is concerned with two of them, and with the nuclear theory that underpins their interpretation.

Nuclear β decay was instrumental in establishing the $V-A$ structure of the weak interaction and remains today one of the most sensitive low-energy probes of the charged-current sector [1,2]. Superallowed $0^+ \to 0^+$ Fermi transitions provide the

most precise determination of the up-down quark mixing matrix element V_{ud} in the Cabibbo–Kobayashi–Maskawa (CKM) matrix, the quantity which dominates the top-row unitarity test $\Delta_{\mathrm{CKM}} = |V_{ud}|^2 + |V_{us}|^2 + |V_{ub}|^2 - 1$ [4,5]. When dispersive evaluations of the single-nucleon electroweak radiative corrections reduced their uncertainty by a factor of two [6], the unitarity measure Δ_{CKM} moved into tension with the SM. At present, the top-row sum falls short of unity at the level of two to three standard deviations (depending on the treatment of the experimental input) and is known as the Cabibbo angle anomaly [5,7]. Beyond the unitarity test, precision measurements of β-spectra and decay correlations probe scalar and tensor interactions that are absent in the SM: per-mille-level bounds on the Fierz interference term translate into sensitivity to new physics above the 10 TeV scale. This is competitive with and complementary to direct collider searches [1,2,8,9].

The precision spectroscopy of light atomic systems offers a second, independent test. Hydrogen-like atoms are among the most well-understood bound states in nature theoretically speaking. Comparisons of their measured and computed level structures test quantum electrodynamics (QED) for composite systems, determine fundamental parameters such as the Rydberg constant, and constrain hypothetical new lepton-nucleus interactions at the femtometer scale [10]. Since the muon is roughly 200 times heavier than the electron, muonic atoms play a special role in this program; nuclear finite-size effects in the spectra are enhanced by the third power of the mass ratio, which makes the muonic Lamb shift the most precise source of absolute nuclear charge radii [11]. The charge radius extracted from muonic hydrogen famously disagreed with the electronic determinations accepted at the time—known as the proton-radius puzzle [12,13], a discrepancy since resolved in favor of the muonic value—and muonic radii now enter the CODATA adjustment of fundamental constants [14]. Confronting muonic with electronic determinations has since developed into a sensitive test of lepton universality, with the recent focus having fallen on the helium-isotope shift. The muonic and electronic values for the difference of the squared charge radii of ^{3}He and ^{4}He were found to disagree at the 3.6σ level [15–17], and a systematic re-evaluation of the nuclear-structure corrections sharpened the tension to 4σ [18]. The discrepancy has since been traced to atomic rather than nuclear theory. Known second-order hyperfine contributions to the electronic isotope shift, previously neglected or treated only approximately, were recently identified and computed [19,20], which brought the two determinations into agreement at the 1.3σ level with respect to Ref. [16], and 1.7σ with respect to Ref. [18]. This turned the helium isotope shift from a puzzle into a stringent consistency test of the muonic-atom program.

In all of these searches, the sensitivity to new physics is limited not by experiment but by nuclear structure theory. In muonic atoms, the QED contributions are under excellent control [21], and the uncertainty of the extracted radii is dominated by the two-photon-exchange (TPE) or $\gamma\gamma$ box correction in which the exchanged virtual photons are sensitive to the full nuclear spectrum [10,22]. In superallowed decays, the nuclear-structure-dependent radiative corrections, particularly the nuclear γW box, were found to be far less controlled than previously assumed once the single-nucleon analysis had been improved. Their re-evaluation inflated the uncertainty in V_{ud} by roughly 50% between the 2015 and 2020 critical surveys [2,4,23,24]. Likewise, interpreting spectrum-shape and correlation measurements at their targeted $\mathcal{O}(10^{-3})$ accuracy requires recoil-order and induced-current nuclear corrections of commensurate precision [1,8,9]. This entire program, therefore, hinges on a single capability: computing amplitudes of electroweak currents in nuclei at the percent level with rigorous uncertainties that admit a statistical interpretation. This is what modern *ab initio* nuclear theory has begun to deliver by combining nuclear Hamiltonians and electroweak currents consistently derived from chiral effective field theory (χEFT) [25–27],

systematically improvable many-body methods [28], and Bayesian uncertainty quantification [29,30].

The theme of this review is that the leading nuclear-structure corrections entering the aforementioned flagship programs are two faces of the same theoretical coin. The relevant object is the forward electroweak current-current correlator with external nuclear states, i.e., the generalized hadronic tensor, as pictured in Figure 1. In muonic atoms both currents are electromagnetic, and the correlator governs the TPE contribution to the Lamb shift. In superallowed β decays, one current is electromagnetic and the other the weak-charged current, and the correlator constitutes the nuclear γW box correction. This kinship was recognized early in the modern reassessment of the radiative corrections, when the sum-rule and Lanczos techniques developed for muonic atoms were identified as the natural tools for the nuclear γW box [1]. It extends to the entire computational chain: the spectral decomposition over nuclear intermediate states, the multipole expansion of the current operators, the Lanczos-based methods giving access to the required response functions and resolvents, and the order-by-order χEFT analysis underlying the uncertainty estimates. The dividends of a unified treatment are visible in two recent milestones, namely (i) the TPE corrections in muonic helium computed with Bayesian inference, which enabled the precise determinations of the helion and α-particle charge radii and exonerated the nuclear-structure corrections in the helium isotope-shift puzzle [18], and (ii) one of the first *ab initio* computations of the nuclear γW box for the lightest superallowed transition, $^{10}\mathrm{C} \to {}^{10}\mathrm{B}$ [31]. The two programs are, moreover, coupled in practice and not only in formalism: the reference charge radii anchoring the superallowed analysis of the $^{26m}\mathrm{Al} \to {}^{26}\mathrm{Mg}$ transition are themselves extracted from muonic X-ray spectroscopy, so that the nuclear polarization correction propagates into the statistical rate function and, ultimately, into V_{ud}. A recent re-analysis along these lines reduced the CKM unitarity deficit by one standard deviation [32].

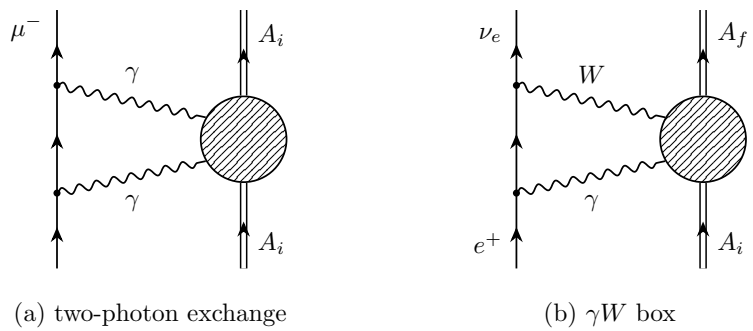

(a) two-photon exchange (b) γW box

Figure 1. Diagrammatic kinship of the two corrections reviewed here: (**a**) two-photon exchange in muonic atoms and (**b**) the γW box in superallowed β decay, drawn for a β^+ transition such as $^{10}\mathrm{C} \to {}^{10}\mathrm{B}$. Thin and double lines denote the leptons and the nucleus, respectively. The hatched blob is the same object in both diagrams, the generalized hadronic tensor, carrying two electromagnetic currents in (**a**) and one electromagnetic and one charged-weak current in (**b**).

In this review, we concentrate on the nuclear-structure-dependent corrections entering the muonic-atom and superallowed programs with a particular focus on light nuclei, where wave-function-based *ab initio* methods provide numerically exact solutions of the many-body problem and rigorous uncertainty quantification is within reach. Heavier systems, for which this level of control is not yet available, are briefly discussed in connection with the recent experimental program in muonic X-ray spectroscopy [33–36]. While not covered in this review, the same machinery underpins the analysis of β-spectra and angular correlations in searches for exotic currents [8,9]. We address the single-nucleon contributions to both observables only insofar as they enter the nuclear analysis [37,38]. Comprehensive

accounts of muonic-atom spectroscopy and its theory may be found in Refs. [10,11,22], of the superallowed data set in Ref. [4] and electroweak radiative corrections to β decay in Ref. [5], and of modern *ab initio* many-body methods in Ref. [28].

The review is organized as follows. In Section 2, we introduce the common theoretical framework: the generalized hadronic tensor, its spectral representation in terms of nuclear eigenstates, and the multipole decomposition of the electroweak current operators. In Section 3, we summarize the state-of-the-art in terms of *ab initio* theory: χEFT Hamiltonians and currents, the many-body and Lanczos-based methods used to compute the relevant amplitudes, and Bayesian uncertainty quantification. In Section 4, we review recent progress in muonic atoms, from the TPE formalism and the associated multipole sum rules to Bayesian-quantified predictions for muonic helium, their impact on the helium isotope-shift puzzle, and developments in heavy muonic atoms. In Section 5, we turn towards superallowed β decays, specializing the hadronic tensor to the γW box, reviewing the first *ab initio* calculations, and discussing the implications for V_{ud} and CKM unitarity. In Section 6, we conclude and discuss anticipated future directions.

2. Common Theory of Nuclear-Structure Corrections

The leading nuclear-structure-dependent corrections introduced in Section 1—the two-photon exchange in muonic atoms and the γW box in superallowed β decays—are both two-boson-exchange amplitudes in which the lepton lines and bosonic propagators factorize into process-dependent kinematic structures, while all nuclear structure is captured by a single object: the generalized hadronic tensor, a forward current-current correlator of electroweak operators evaluated with external nuclear states, nowadays accessible with *ab initio* many-body theory. Throughout, we work in natural units ($\hbar = c = 1$) with unit-normalized nuclear states, matching with the relativistic normalization of amplitudes employed in the β-decay literature is discussed in Section 5. In Section 2.1, we define the generalized hadronic tensor and derive its spectral representation in terms of nuclear eigenfunctions. In Section 2.2, we decompose the electroweak current operators into multipoles, the most pragmatic form in which nuclear amplitudes of currents are evaluated.

2.1. The Hadronic Tensor and Current-Current Correlators

The probes considered in this review couple with the nucleus through electromagnetic and charged weak currents, which, for the two lightest quark degrees of freedom, read

$$J^{\mu}_{\rm em} = \frac{2}{3}\bar{u}\gamma^{\mu}u - \frac{1}{3}\bar{d}\gamma^{\mu}d \qquad\qquad J^{\dagger\,\mu}_{\rm W} = \bar{d}\,\gamma^{\mu}\left(1-\gamma_5\right)u. \tag{1}$$

At the energies relevant to nuclear structure, however, one does not work with quark degrees of freedom. The nuclear amplitudes of the above currents are evaluated with effective operators derived from chiral effective field theory (χEFT) and formulated in terms of nucleon and pion degrees of freedom; the operators are organized into one- and many-body contributions and are constructed consistently with the nuclear interaction [39], as discussed in Section 3.1. The quark-level expressions fix the relevant charges, isospin structure, and vector or axial-vector nature of the probes that the effective operators realize at low energies. With the current operators understood in this effective sense, and introducing the momentum-space current $J^{\mu}_{X}(t,\mathbf{q}) = \int d^3x\, e^{-i\mathbf{q}\cdot\mathbf{x}}\, J^{\mu}_{X}(t,\mathbf{x})$, we define the generalized non-relativistic hadronic tensor with unit-normalized external states as

$$H^{\mu\nu}_{XY}(q;f,i) \equiv -i\int dt\, e^{iq_0t}\langle f|T\left\{J^{\mu}_{X}(t,\mathbf{q})J^{\nu}_{Y}(0,-\mathbf{q})\right\}|i\rangle + B^{\mu\nu}_{XY}(\mathbf{q};f,i), \tag{2}$$

where X and Y label the currents and external probes. For example, $X, Y = \text{em}$ corresponds to the electromagnetic two-photon-exchange problem, while $X = \text{em}$ and $Y = \text{W}$ corresponds to the electroweak current-current correlator relevant to radiative corrections in β decay. The term $B^{\mu\nu}_{XY}$ denotes the possible two-boson contact, or seagull, contributions. Finally, $|i\rangle$ and $|f\rangle$ are eigenstates of the nuclear Hamiltonian. Both current insertions in Equation (2) are Fourier-transformed with respect to their spatial arguments and carry opposite three-momenta, $\mathbf{q}$ and $-\mathbf{q}$, so that no net three-momentum is transferred to the external nucleus; the remaining integral is the transform with respect to the relative time separation of the two insertions. The overall normalization is a matter of convention and is chosen here such that the spectral representation provided below has the same structure as utilized in the muonic-atom two-photon-exchange formalism (in β-decay literature there is additional factor of $1/2$ in the normalization of the relativistic tensor).

For applications to nuclear many-body theory, it is useful to evaluate Equation (2) in terms of nuclear eigenstates. We express the momentum-space current defined above in the Heisenberg picture with H_{nuc} the nuclear Hamiltonian as

$$J^{\mu}_{X}(t, \mathbf{q}) = e^{iH_{\text{nuc}}t} J^{\mu}_{X}(\mathbf{q}) e^{-iH_{\text{nuc}}t} \qquad H_{\text{nuc}}|N\rangle = E_N|N\rangle. \tag{3}$$

One then expands the time-ordered product, resolves the intermediate nuclear spectrum, and performs the remaining t integration to yield

$$\begin{aligned} H^{\mu\nu}_{XY}(q; f, i) \quad = \quad & \sum_N \frac{\langle f|J^{\mu}_{X}(\mathbf{q})|N\rangle\langle N|J^{\nu}_{Y}(-\mathbf{q})|i\rangle}{E_f - E_N + q_0 + i\epsilon} + \sum_N \frac{\langle f|J^{\nu}_{Y}(-\mathbf{q})|N\rangle\langle N|J^{\mu}_{X}(\mathbf{q})|i\rangle}{E_i - E_N - q_0 + i\epsilon} \\ & + B^{\mu\nu}_{XY}(\mathbf{q}; f, i), \end{aligned} \tag{4}$$

which is the form most amenable to nuclear response and sum rule calculations in *ab initio* theory. It also clarifies that all nuclear structure enters via the intermediate spectrum of H_{nuc} and the corresponding transition amplitudes of the electroweak current operators.

At this point, it is useful to clarify the meaning of "forward". In the language of scattering theory, a forward tensor refers to kinematics with no overall momentum transfer to the external target. This is manifest in Equation (4), where the two current insertions carry opposite momenta, $\mathbf{q}$ and $-\mathbf{q}$, so that no net three-momentum is transferred to the external nucleus. For the electromagnetic two-photon-exchange problem in muonic atoms, the external initial and final nuclear states are identical, $|i\rangle = |f\rangle$, and the tensor is an elastic forward electromagnetic correlator. For superallowed β decay, the external nuclear states are instead connected by the weak transition and are not identical. In that case, the corresponding object is a transition current-current correlator.

In the non-relativistic theory, the center-of-mass motion separates exactly from the intrinsic dynamics, and, since the two current insertions carry opposite three-momenta, momentum conservation fixes the center-of-mass momentum of the intermediate states to $\mp\mathbf{q}$ relative to the external nucleus. The eigenvalues E_N entering the denominators of Equation (4) then contain, in addition to the intrinsic energies of the nuclear eigenstate with mass M_N, the center-of-mass energy $\mathbf{q}^2/2M_N$ of the recoiling intermediate nucleus. Further, all non-relativistic amplitudes of current operators reduce to intrinsic amplitudes. Whether this recoil shift of the pole positions is retained depends on the accuracy sought. It is kept explicitly in the γW box analysis of Section 5, whereas, in the muonic-atom application, it is suppressed by the lepton-to-nucleus mass ratio and does not enter the leading multipole sum rules of Section 4.

For the electromagnetic two-photon-exchange problem relevant to muonic atoms, one sets $X = Y = \text{em}$ and $|i\rangle = |f\rangle = |0\rangle$. The generalized tensor then reduces to

$$H^{\mu\nu}_{\text{em}\,\text{em}}(q;0,0) = \sum_N \frac{\langle 0|J^\mu_{\text{em}}(\mathbf{q})|N\rangle\langle N|J^\nu_{\text{em}}(-\mathbf{q})|0\rangle}{E_0 - E_N + q_0 + i\epsilon} + \sum_N \frac{\langle 0|J^\nu_{\text{em}}(-\mathbf{q})|N\rangle\langle N|J^\mu_{\text{em}}(\mathbf{q})|0\rangle}{E_0 - E_N - q_0 + i\epsilon} + B^{\mu\nu}_{\text{em}\,\text{em}}(\mathbf{q}), \tag{5}$$

the elastic forward electromagnetic tensor evaluated with (the same) external nuclear ground states; this process is to be discussed in Section 4.

For the electroweak radiative corrections to superallowed β decay, the relevant object contains one electromagnetic and one charged weak current. Taking $X = \text{em}$ and $Y = \text{W}$ in Equation (4), one obtains

$$H^{\mu\nu}_{\text{em}\,\text{W}}(q;f,i) = \sum_N \frac{\langle f|J^\mu_{\text{em}}(\mathbf{q})|N\rangle\langle N|J^\nu_{\text{W}}(-\mathbf{q})|i\rangle}{E_f - E_N + q_0 + i\epsilon} + \sum_N \frac{\langle f|J^\nu_{\text{W}}(-\mathbf{q})|N\rangle\langle N|J^\mu_{\text{em}}(\mathbf{q})|i\rangle}{E_i - E_N - q_0 + i\epsilon} + B^{\mu\nu}_{\text{em}\,\text{W}}(\mathbf{q}), \tag{6}$$

where $|i\rangle$ and $|f\rangle$ denote the initial and final nuclear states connected by the weak transition. Note that these states are not necessarily the ground states of a given system. For spin-zero external states, as in superallowed $0^+ \to 0^+$ Fermi transitions, the vector–axial–vector part of this tensor can be projected onto a single scalar amplitude denoted by T_3. It is to be discussed in Section 5, along with a comment on the nature of $B^{\mu\nu}_{\text{em}\,\text{W}}(\mathbf{q})$ in the context of the γW box correction.

2.2. Multipoles of Current Operators

The spectral representation of the hadronic tensor introduced in Section 2.1 is written in terms of amplitudes of momentum-space electroweak current operators. In practical *ab initio* calculations, these currents are usually expanded in multipoles and thus decomposed into a sum over rank-J irreducible tensor operators. This provides a systematic expansion that separates away the angular dependence of the current and allows for a simple truncation scheme in the number of multipolar contributions. We separate the Minkowski-space current into its time and space components,

$$J^\mu_X(q) = (\rho_X(q), \mathbf{J}_X(q)), \tag{7}$$

where $\rho_X \equiv J^0_X$ is the nuclear charge-density operator, and $\mathbf{J}_X$ is the nuclear current-density operator. The following decomposition applies equally to the electromagnetic and weak currents, albeit with proper accounting for γ_5 and changes in the single-nucleon form factors. Following the standard multipole formalism for semi-leptonic weak and electromagnetic interactions with nuclei [40,41], and choosing the quantization axis along the $\mathbf{q}$ direction, the charge density and the spatial current decompose into irreducible tensor operators (thus with definite angular momentum and parity) as

$$\rho_X(\mathbf{q}) = \sqrt{4\pi} \sum_{J=0}^{\infty} (-i)^J \sqrt{2J+1}\, M_{X,J0}(\mathbf{q}), \tag{8}$$

and

$$\mathbf{J}_X(\mathbf{q}) = \sqrt{4\pi}\sum_{J=0}^{\infty}(-i)^J\sqrt{2J+1}\,L_{X,J0}(\mathbf{q})\,\hat{\mathbf{e}}_0(\hat{\mathbf{q}}) + \sqrt{2\pi}\sum_{\lambda=\pm1}\sum_{J=1}^{\infty}(-i)^J\sqrt{2J+1}\Big[T^{\rm el}_{X,J\lambda}(\mathbf{q}) - \lambda\,T^{\rm mag}_{X,J\lambda}(\mathbf{q})\Big]\hat{\mathbf{e}}^*_\lambda(\hat{\mathbf{q}}), \tag{9}$$

where $\hat{\mathbf{e}}_0(\hat{\mathbf{q}}) = \hat{\mathbf{q}}$ and $\hat{\mathbf{e}}_{\pm1}$ are the transverse spherical unit vectors. Equations (8) and (9) follow by insertion of the multipole expansion of the plane wave $e^{-i\mathbf{q}\cdot\mathbf{x}}$ in the Fourier transform of the current operators. The four operators $M_{X,JM}$, $L_{X,JM}$, $T^{\rm el}_{X,JM}$, and $T^{\rm mag}_{X,JM}$ are the Coulomb, longitudinal, transverse electric, and transverse magnetic multipoles, in the standard naming of Refs. [40,41].

The multipoles are projections of the nuclear charge and current densities onto a given basis of functions

$$M_{X,JM}(\mathbf{q}) = \int d^3x\, j_J(|\mathbf{q}||\mathbf{x}|)\,Y_{JM}(\hat{\mathbf{x}})\,\rho_X(\mathbf{x}), \tag{10}$$

$$L_{X,JM}(\mathbf{q}) = \frac{i}{|\mathbf{q}|}\int d^3x\,\Big[\nabla\, j_J(|\mathbf{q}||\mathbf{x}|)\,Y_{JM}(\hat{\mathbf{x}})\Big]\cdot\mathbf{J}_X(\mathbf{x}), \tag{11}$$

$$T^{\rm el}_{X,JM}(\mathbf{q}) = \frac{1}{|\mathbf{q}|}\int d^3x\,\Big[\nabla\times j_J(|\mathbf{q}||\mathbf{x}|)\,\mathbf{Y}_{JJM}(\hat{\mathbf{x}})\Big]\cdot\mathbf{J}_X(\mathbf{x}), \tag{12}$$

$$T^{\rm mag}_{X,JM}(\mathbf{q}) = \int d^3x\, j_J(|\mathbf{q}||\mathbf{x}|)\,\mathbf{Y}_{JJM}(\hat{\mathbf{x}})\cdot\mathbf{J}_X(\mathbf{x}), \tag{13}$$

where j_J is a spherical Bessel function, and Y_{JM} and $\mathbf{Y}_{JJM}$ are the spherical and vector spherical harmonics, respectively. The single-particle reduced amplitudes of the multipole operators are known and tabulated in the harmonic-oscillator basis [41] and available symbolically for arbitrary quantum numbers [42]. The four operators above exhaust the multipole content of the electromagnetic current. However, since the charged-weak current has a $V-A$ structure, there exists an additional axial-vector multipole for each vector-current multipole listed above. We denote these multipoles by the superscript "5", for example, $T^{5,\rm el}_{W,JM}$ or $T^{5,\rm mag}_{W,JM}$, and note that they carry parity opposite to their vector counterparts and enter the γW box multipole sum of Section 5.

For conserved vector currents, the Coulomb and longitudinal multipoles are related by the continuity equation. In momentum space, current conservation implies

$$q_0\,\rho_X(\mathbf{q}) = \mathbf{q}\cdot\mathbf{J}_X(\mathbf{q}), \tag{14}$$

where q_0 is fixed by the amplitude under consideration. This fixes the longitudinal multipole in terms of the Coulomb one as

$$L_{X,JM}(q) = \frac{q_0}{q}\,M_{X,JM}(q). \tag{15}$$

This relation is routinely used to simplify electromagnetic response calculations. The axial-vector current, by contrast, is not conserved, and the corresponding longitudinal multipole must be retained explicitly [40].

3. Modern *Ab Initio* Methods

The common formalism introduced in Section 2 reduces the hadronic-structure-dependent corrections of interest to amplitudes and response functions involving electroweak currents in nuclei. This section summarizes the ingredients from *ab initio* theory needed to evaluate these quantities in practical situations. In Section 3.1, we discuss nuclear Hamiltonians, electroweak current operators, and the many-body methods used to compute the relevant amplitudes. Section 3.2 then describes how Lanczos techniques can be used to access the response functions and sum rules entering the hadronic tensor. Finally,

Section 3.3 reviews recent developments in uncertainty quantification, with a particular emphasis on the propagation of χEFT truncation errors.

3.1. Nuclear Hamiltonians, Electroweak Operators and Ab Initio Theory

Microscopic inputs to the hadronic tensor consist of a chosen nuclear Hamiltonian, a basis of electroweak current operators, and a many-body method capable of evaluating the required ground-state and transition amplitudes. In an *ab initio* approach, these ingredients are constructed within a common theoretical framework and are then applied to observables for a given process without further adjustment. This consistency is essential for the applications discussed in this review.

Historically, quantitative nuclear-structure calculations relied heavily on high-precision phenomenological interactions. The development of accurate nucleon-nucleon (NN) potentials, such as Argonne v18 (AV18) [43] and CD-Bonn [44], supplemented by phenomenological three-nucleon (3N) interactions such as the Urbana IX and Illinois models [45,46], enabled a highly successful description of the properties of light nuclei. Constructed to reproduce NN scattering data and selected few-body observables with high accuracy, they established the predictive power of modern few-body calculations. Their empirical nature, however, left them without a systematic low-energy expansion of Quantum Chromodynamics (QCD), a controlled hierarchy of many-body forces, or a natural prescription for propagating theoretical uncertainties.

A major conceptual advance came with Weinberg's proposal to formulate nuclear forces within effective field theory [47–49]. Chiral effective field theory (χEFT) has since become the standard framework for constructing nuclear Hamiltonians consistent with the symmetries of low-energy QCD [25–27]. In this approach, the relevant degrees of freedom are nucleons and pions, while unresolved short-distance physics is encoded in low-energy constants (LECs) that are constrained by experimental data. The resulting nuclear Hamiltonian takes the schematic form

$$H_{\rm nuc} = T_{\rm rel} + V_{\rm NN} + V_{\rm 3N} + V_{\rm 4N} + \cdots , \tag{16}$$

where $T_{\rm rel}$ is the relative kinetic energy and the nuclear interactions are organized according to the chiral expansion. In Weinberg's power counting, the leading-order Hamiltonian only contains NN forces, 3N forces emerge at next-to-next-to-leading order (N^{2}LO), and 4N forces arise at higher orders [25,26]. Modern chiral interactions have reached a high level of sophistication. Two-nucleon forces have been derived to high orders in the chiral expansion, including N^{4}LO and partial N^{5}LO contributions [50,51]. At the same time, the role of the $\Delta(1232)$ nucleon resonance has motivated the development of Δ-full formulations, in which the Δ is included as an explicit degree of freedom. This can improve the convergence pattern of the chiral expansion by incorporating important intermediate-range physics at lower orders [25,26,52].

Despite this progress, the formulation and use of chiral interactions involve important conceptual and practical issues. Chiral potentials are singular at short distances and must be regularized before they can be iterated in the Schrödinger equation. In the standard implementation of Weinberg's power counting, the cutoff is kept finite and chosen to be of the order of the EFT breakdown scale. Observables, therefore, retain a residual cutoff dependence, which should decrease systematically as higher orders are included. An alternative strategy emphasizes strict renormalization-group invariance and treats sub-leading interactions perturbatively after solving the leading-order problem non-perturbatively [27,53,54]. The relation between these approaches, and the extent to which they provide controlled order-by-order convergence in nuclei, remains an active area of research.

The regulator structure of chiral interactions also matters for many-body calculations. Many chiral potentials are naturally formulated in momentum space and are non-local. This can be challenging for coordinate-space methods, particularly Quantum Monte Carlo (QMC) approaches. A significant effort has, therefore, been devoted to constructing local or maximally local chiral interactions suitable for coordinate-space calculations [55–58]. By exploiting regulator choices and Fierz rearrangement freedom, local NN interactions have been developed to high chiral orders, and local 3N forces have been implemented through N^2LO [56,58]. These interactions have enabled QMC calculations of light nuclei and neutron matter, and they are also useful in other coordinate-space approaches, such as hyperspherical harmonics calculations [59].

For the observables discussed in this review, the Hamiltonian alone is not sufficient. The hadronic tensor in Equation (4) also depends on electromagnetic and weak current operators. These operators must be constructed consistently with the nuclear interaction. In χEFT, electroweak currents are organized in the same low-energy expansion as the nuclear forces and contain both one-body and many-body contributions [39]. Schematically,

$$J_X^\mu = \sum_i J_{X,i}^{\mu,1\mathrm{b}} + \sum_{i<j} J_{X,ij}^{\mu,2\mathrm{b}} + \cdots , \tag{17}$$

where $X = \mathrm{em}$ (electromagnetic) or W (weak), and the ellipsis denotes higher-body current operators. The one-body term, in which the external probe couples to individual nucleons, contains the leading impulse approximation currents. Two-body currents encode mechanisms in which the probe couples to correlated nucleon pairs, and they include meson-exchange effects. These terms are required by current conservation for consistency with the nuclear Hamiltonian.

The quantitative impact of two-body electroweak currents has been demonstrated in a variety of few-body observables. For many weak transitions in light nuclei, the one-body impulse approximation accounts for the dominant contribution, while two-body axial currents provide smaller but non-negligible corrections [9,60,61]. Some transitions exhibit enhanced sensitivity: in selected $A = 8$ β decays [61], the leading one-body Gamow-Teller matrix element is suppressed by approximate Wigner spin-isospin symmetry, making the relative effect of two-body currents unusually large [62].

Once the Hamiltonian and electroweak current operators are specified, the remaining task is to solve the nuclear many-body problem and evaluate the amplitudes entering the spectral representation of the hadronic tensor. In light nuclei, methods such as Quantum Monte Carlo [63–65], Hyperspherical Harmonics (HH) [66,67], their variants such as the Effective Interaction Hyperspherical Harmonics (EIHH) [59,68], and the No-Core Shell Model (NCSM) [69] can provide highly accurate solutions of the Schrödinger equation and detailed access to nuclear correlations. In medium-mass nuclei, many-body frameworks such as Coupled Cluster (CC) [70] and In-Medium Similarity Renormalization Group (IMSRG) [71] extend the reach of *ab initio* calculations to heavier systems via controlled, polynomial-scaling approximations. A broad overview of modern *ab initio* methods may be found in Ref. [28].

3.2. The Lanczos Algorithm

In this section, we review the Lanczos methods fundamental to calculations in configuration interaction theory. We will denote a general discretized Hamiltonian represented in a truncated configuration space basis of dimension d as $\bar{H} \equiv \bar{H}(d)$ and note that $\lim_{d\to\infty} \bar{H}(d) = H$ in the weak sense (meaning the spectrum $\sigma(H)$ is recovered). Then,

$$\bar{H}(d) = \begin{pmatrix} \langle \psi_1^A | H | \psi_1^A \rangle & \cdots & \langle \psi_1^A | H | \psi_d^A \rangle \\ \vdots & \ddots & \vdots \\ \langle \psi_d^A | H | \psi_1^A \rangle & \cdots & \langle \psi_d^A | H | \psi_d^A \rangle \end{pmatrix}, \tag{18}$$

and the work to be done is that of matrix algebra; given the typical dimensions d, one must apply approximate diagonalization schemes to construct the eigensolutions of $\bar{H}(d)$.

For a given Hermitian operator, the most powerful such approach is the Lanczos algorithm [72,73] which is premised on the existence of a special basis in which the matrix $\bar{H}(d)$ has tri-diagonal form. A Krylov method, the Lanczos algorithm iteratively generates an orthonormal basis from recursive application of the desired operator on a random starting vector, called the pivot, which has non-zero overlap with the desired part of the spectrum. In practice, the number of algorithm iterations N_{iter} is guided by the characteristics of the spectrum in question, e.g., (i) the eigenvalue density, (ii) the number of desired converged eigensolutions, (iii) the number of degrees of freedom, and (iv) the dimension d. While completion of the algorithm with $N_{\text{iter}} = d$ is typically not possible, the remarkable advantage of the Lanczos algorithm is that one needs a number of iterations far less than the dimension of the matrix in most scenarios of interest, i.e., $N_{\text{iter}} \ll d$. The conditions on convergence were already well-understood in his time by Lanczos [72], yet more recent studies have elucidated further details on bounds of the Lanczos-type methods; see Ref. [74] and the references therein, as well as Ref. [75].

Formally initialized from a random, normalized pivot vector $|\eta_0\rangle$—though vectors bootstrapped from lower-dimensional configuration spaces offer a pragmatic convergence-accelerating alternative—we generate a sequence of Lanczos basis vectors $\{|\eta_i\rangle\}$ for a Hermitian operator, $\bar{H}$, as

$$\begin{aligned} \bar{H}|\eta_0\rangle &= \alpha_0 |\eta_0\rangle + \beta_0 |\eta_1\rangle \\ \bar{H}|\eta_1\rangle &= \beta_0 |\eta_0\rangle + \alpha_1 |\eta_1\rangle + \beta_1 |\eta_2\rangle \\ \bar{H}|\eta_2\rangle &= \qquad\qquad \beta_1 |\eta_1\rangle + \alpha_2 |\eta_2\rangle + \beta_2 |\eta_3\rangle \\ \bar{H}|\eta_3\rangle &= \qquad\qquad\qquad\qquad \beta_2 |\eta_2\rangle + \alpha_3 |\eta_3\rangle + \beta_3 |\eta_4\rangle \\ &\vdots \end{aligned}$$

where each new vector in the sequence is constructed to be explicitly orthonormal to its two leftmost neighbors (further re-orthogonalization against the whole sequence via the Gram–Schmidt procedure is often necessary) as

$$\beta_i |\eta_{i+1}\rangle = \bar{H}|\eta_i\rangle - \alpha_i |\eta_i\rangle - \beta_{i-1} |\eta_{i-1}\rangle, \tag{19}$$

$$\alpha_i = \langle \eta_i | \bar{H} | \eta_i \rangle \qquad \beta_i^2 = \left|\left| (\bar{H} - \alpha_i \mathbb{1}) |\eta_i\rangle - \beta_{i-1} |\eta_{i-1}\rangle \right|\right|_{L^2}^2. \tag{20}$$

The Lanczos basis spans the Krylov subspace generated by the pivot vector and $\bar{H}$, that is,

$$\mathcal{K}_{N_{\text{iter}}}(\eta_0, \bar{H}) \equiv \text{span}\Big\{ |\eta_0\rangle, \bar{H}|\eta_0\rangle, \bar{H}^2|\eta_0\rangle, \ldots, \bar{H}^{N_{\text{iter}}-1}|\eta_0\rangle \Big\},$$

and casts an $N_{\text{iter}} \times N_{\text{iter}}$ sub-block of $\bar{H}$ into tri-diagonal form, which we denote as $\bar{H}_{\text{L}}$. Thus, the Rayleigh–Ritz eigensolutions of $\bar{H}$ are given entirely in terms of the generated set of coefficients $\{\alpha_i, \beta_i\}$ and the Lanczos vectors $\{|\eta_i\rangle\}$ as

$$E \doteq P^{-1}\bar{H}_{\mathrm{L}}\,P \qquad \left|\Psi_i\right\rangle \doteq \sum_{j=1}^{N_{\mathrm{iter}}} \left\langle \eta_j \middle| \Psi_i \right\rangle \left|\eta_j\right\rangle = \sum_{j=1}^{N_{\mathrm{iter}}} \left(P^{-1}\right)_{ij} \left|\eta_j\right\rangle = \sum_{j=1}^{N_{\mathrm{iter}}} P_{ji} \left|\eta_j\right\rangle, \tag{21}$$

where P denotes the $N_{\mathrm{iter}} \times N_{\mathrm{iter}}$ unitary matrix containing the coordinates of the Rayleigh–Ritz eigenvectors in the Lanczos basis.

Let us now consider a problem in which we have a bounded Hamiltonian operator, $\bar{H}$, and we would like to evaluate amplitudes of the following form:

$$\mathcal{A}_{fi} = \left\langle \Psi_f \right| \bar{O}_2 \left(z - \bar{H}\right)^{-1} \bar{O}_1 \left|\Psi_i\right\rangle = \left\langle \Psi_f \right| \bar{O}_2 \left|\Psi_{\mathrm{R}}\right\rangle, \tag{22}$$

$$\left(z - \bar{H}\right) \left|\Psi_{\mathrm{R}}\right\rangle = \bar{O}_1 \left|\Psi_i\right\rangle, \tag{23}$$

where $z \in \mathbb{C} \setminus \sigma(\bar{H})$. Without loss of generality, we will assume that $\bar{O}_1$ and $\bar{O}_2$ are irreducible spherical tensor operators that carry good spin-parity numbers, and we note that any relevant operator may be projected onto good spin-parity via an expansion akin to the multipole decomposition given in Section 2.2. One clearly recognizes that Equation (23) is an inhomogeneous Schrödinger equation with a source given by the action of $\bar{O}_1$ on the initial state and, almost exactly as in the homogeneous case, the solutions may be constructed via the Lanczos algorithm. Remarkably, though, the admitted solutions will contain information about transitions to the entire spectrum relevant to construction of the Green function in the desired amplitude,

$$\mathcal{A}_{fi} = \sum\!\!\!\!\!\!\int_n \frac{\left\langle \Psi_f \right| \bar{O}_2 \left|\Psi_n\right\rangle \left\langle \Psi_n \right| \bar{O}_1 \left|\Psi_i\right\rangle}{z - \omega_n}, \tag{24}$$

where ω_n denotes the eigenvalue of $\bar{H}$ associated with the eigensolution $\left|\Psi_n\right\rangle$. The formal aspects of this problem have been studied over several decades, e.g., see the early ideas developed for the "recursion method" as applied in condensed matter physics in the works of Haydock, Heine and Kelly [76–80], as well as the 1987 proceedings in Ref. [81]. Moreover, the *ab initio* nuclear theory community has exploited this technique over the last two decades [82–86], with a recent application to electroweak radiative corrections in superallowed beta decays [31].

Modification to the Lanczos algorithm occurs due to the presence of the inhomogeneity; rather than a random pivot, one sets the starting vector to be the normalized constraint

$$\left|\eta_0\right\rangle = \frac{1}{\sqrt{\left\langle \Psi_i \right| \bar{O}_1^\dagger \bar{O}_1 \left|\Psi_i\right\rangle}} \bar{O}_1 \left|\Psi_i\right\rangle. \tag{25}$$

Then, following Ref. [87], we may explicitly construct the desired transition amplitudes in Equation (24) by expansion of the intermediate eigensolutions Ψ_n in the Lanczos basis, by definition given by $\left|\Psi_n\right\rangle = \sum_m c_{nm} \left|\eta_m\right\rangle$. The relevant amplitudes are then

$$\begin{aligned} \left\langle \Psi_n \right| \bar{O}_1 \left|\Psi_i\right\rangle &= \sqrt{\left\langle \Psi_i \right| \bar{O}_1^\dagger \bar{O}_1 \left|\Psi_i\right\rangle} \left\langle \eta_n \right| P^\dagger \left|\eta_0\right\rangle, \\ \left\langle \Psi_f \right| \bar{O}_2 \left|\Psi_n\right\rangle &= \sqrt{\left\langle \Psi_f \right| \bar{O}_2^\dagger \bar{O}_2 \left|\Psi_f\right\rangle} \sum_m \left\langle \eta_m \right| P \left|\eta_n\right\rangle \left\langle \zeta_0 \middle| \eta_m \right\rangle, \end{aligned} \tag{26}$$

where we recall P from Equation (21) to be the unitary matrix which diagonalizes the $N_{\mathrm{iter}} \times N_{\mathrm{iter}}$ tri-diagonal sub-block of the Hamiltonian represented in the Lanczos basis.

In fact, one may trivially evaluate generalized quantities with the above amplitudes of the form

$$I_{fi} = \int dz \, \langle \Psi_f | \, \bar{O}_2 \, f(z, \bar{H}) \, \bar{O}_1 \, | \Psi_i \rangle = \sum\!\!\!\!\!\!\int_n dz \, f(z, \omega_n) \, \langle \Psi_f | \, \bar{O}_2 \, | \Psi_n \rangle \, \langle \Psi_n | \, \bar{O}_1 \, | \Psi_i \rangle, \tag{27}$$

subject to the analytic properties of the function f and the choice of N_{iter} [80,87,88]; by construction, the first $N_{\text{iter}} - 1$ terms of the Taylor series of $f(z, \bar{H})$ are exact. Note that the amplitudes $\mathcal{A}_{fi}$ used to motivate this section are merely a simple case with the choice of analytic function $f(z, \bar{H}) = (z - \bar{H})^{-1}$ on the domain $\mathbb{C} \setminus \sigma(\bar{H})$.

3.3. Uncertainty Quantification

A distinguishing advantage of chiral effective field theory (χEFT) is that it provides not only a systematic framework for constructing nuclear forces and electroweak operators but also a statistically rigorous setting for estimating theoretical uncertainties. In practical applications, the dominant source of theory uncertainty is often the truncation of the chiral expansion at finite order. Such errors were historically estimated heuristically, for example, from the size of the last computed correction or from variations of the regulator scale. The use of Bayesian statistics has since emerged as the gold standard for quantifying EFT truncation errors in a way that is transparent and statistically interpretable [29,30,89,90].

The starting point is the EFT expansion of a generic observable X, computed at chiral order k. The prediction $X^{(k)}$ can be parameterized in terms of a dimensionless expansion parameter Q, typically taken as $Q = \max(p, m_\pi)/\Lambda_b$, where p denotes a characteristic momentum scale of the process and Λ_b is the EFT breakdown scale [29,30,89,91,92]. One then writes

$$X^{(k)} = X_{\text{ref}} \sum_{n=0}^{k} c_n Q^n \qquad X = X^{(k)} + \Delta_k, \tag{28}$$

where X_{ref} sets the overall dimensionful scale, the c_n are dimensionless expansion coefficients, and

$$\Delta_k = X_{\text{ref}} \sum_{n=k+1}^{\infty} c_n Q^n, \tag{29}$$

denotes the residual truncation error. The coefficients c_n can be extracted recursively from the order-by-order results. The core EFT assumption is that, once the relevant scales have been factored out, these coefficients are natural, i.e., typically of order unity.

Bayesian uncertainty quantification translates this naturalness assumption into prior probability distributions for the unknown coefficients, often formulated in terms of an underlying scale parameter $\bar{c}$ that characterizes their typical size. Bayes's theorem is then used to update this prior information using the known coefficients $\{c_0, \ldots, c_k\}$. Marginalizing over $\bar{c}$ yields a posterior probability distribution for the truncation error Δ_k. A major result of this framework was that several older, truncation-error prescriptions were able to be understood as particular, and sometimes overly restrictive, choices of a Bayesian prior [29]. The resulting interval acquires a strict degree-of-belief (DOB) interpretation: conditional on the EFT model and the adopted priors, a 68% DOB interval contains the exact result with 68% probability.

For observables that depend on external kinematic variables, e.g., scattering energy, scattering angle, or momentum transfer, uncertainties at neighboring points are generally correlated. A point-wise application of the Bayesian framework ignores this information and may, therefore, produce unphysical, jagged uncertainty bands. This issue was addressed in Ref. [30], where the EFT coefficients $c_n(x)$ were modeled as draws from a Gaussian process. The resulting formalism incorporates a covariance kernel that encodes the expected smoothness and correlation structure of the observable across the relevant

domain. This yields statistically correlated uncertainty bands and a full covariance matrix for use in fits, hypothesis testing, and diagnostics of the EFT convergence pattern.

While the quantification of truncation errors has seen widespread adoption, a complete theoretical uncertainty quantification (UQ) framework must also account for the statistical uncertainties in the determination of the low-energy constants (LECs) of χEFT. The LECs are typically calibrated to experimental data, such as nucleon-nucleon scattering phase shifts and selected few-nucleon observables. Bayesian parameter estimation provides a rigorous methodology for extracting the joint posterior distribution of these parameters, including their uncertainties and correlations [90,93–95]. Propagating these parameter uncertainties to observables requires repeated solution of the many-body Schrödinger or Lippmann–Schwinger equation and is, therefore, computationally demanding. For this reason, modern nuclear theory has increasingly turned to reduced-order models, or emulators, as part of a broader statistical-computing strategy for uncertainty quantification [90]. In this context, eigenvector continuation (EC), originally introduced as a variational method for tracking eigenvectors in parameter-dependent Hamiltonians [96], has emerged as a particularly promising emulator strategy for nuclear many-body observables, providing efficient and accurate emulation in multi-nucleon systems [95,97,98]. Rigorous Bayesian sampling of the LECs has not yet been applied to nuclear polarizabilities in muonic atoms or to radiative corrections in superallowed β decays; coupling EC-based emulators to electroweak transition amplitudes is the natural next step.

For the applications discussed in this review, the principal source of EFT uncertainty stems from the truncation of the chiral expansion in the nuclear Hamiltonian and in the electroweak current operators, which have to be propagated through the many-body calculation to the final response functions and transition amplitudes [89,99].

4. Recent Progress in Muonic Atoms

A muonic atom is a hydrogen-like bound system in which a negative muon replaces the atomic electron. Because the muon is about 207 times heavier than the electron, its Bohr radius is correspondingly smaller and its wavefunction overlaps far more extensively with the nuclear charge distribution. Nuclear-structure effects in muonic atoms scale as $(m_\mu/m_e)^3$ relative to ordinary atoms and are, therefore, enormously enhanced, turning muonic atoms into precision probes of nuclear structure [11]. This sensitivity is the basis of the experimental program of the CREMA collaboration at the Paul Scherrer Institute, which has measured the $2S$–$2P_{1/2}$ Lamb shift by laser spectroscopy in muonic hydrogen [12,13], muonic deuterium [100], and the muonic helium ions $\mu^3\mathrm{He}^+$ and $\mu^4\mathrm{He}^+$ [15,16].

4.1. Physical Context and Observables

The extraction of nuclear radii from spectroscopic measurements in atomic systems originates from a careful comparison with precise theoretical predictions. The measured Lamb shift in a muonic atom can be parametrized as

$$\delta_{\mathrm{LS}} = \delta_{\mathrm{QED}} + \mathcal{A}_{\mathrm{OPE}}\, r_c^2 + \delta_{\mathrm{NS},\mu}\,, \tag{30}$$

where δ_{QED} collects the purely quantum-electrodynamical and recoil contributions; see Ref. [10] for a recent summary of these contributions. The second term is the leading finite-size effect: it arises from one-photon exchange with the nuclear charge form factor inserted at the photon–nucleus vertex, and is proportional to the mean-square charge radius r_c^2 through the known coefficient $\mathcal{A}_{\mathrm{OPE}} \simeq m_r^3(Z\alpha)^4/12$, with m_r being the muon–nucleus reduced mass. The charge radius is the quantity of interest and is extracted by equating Equation (30) to the spectroscopic measurement once δ_{QED} and $\delta_{\mathrm{NS},\mu}$ are known.

The last term, $\delta_{\mathrm{NS},\mu}$, includes nuclear structure effects which require knowledge of the full nuclear dynamics; the subscript μ distinguishes it from the analogous nuclear-structure correction δ_{NS} entering superallowed β decay (Section 5). Its leading-order contribution is the radiative two-photon-exchange nuclear-structure correction δ_{TPE}, of order $(Z\alpha)^5$; see Figure 2. While δ_{QED} is known to achieve high accuracy, and the spectroscopic measurements are extremely precise, δ_{TPE} is more difficult to calculate; it is by far the dominant source of uncertainty in the extracted radii [10,11,22].

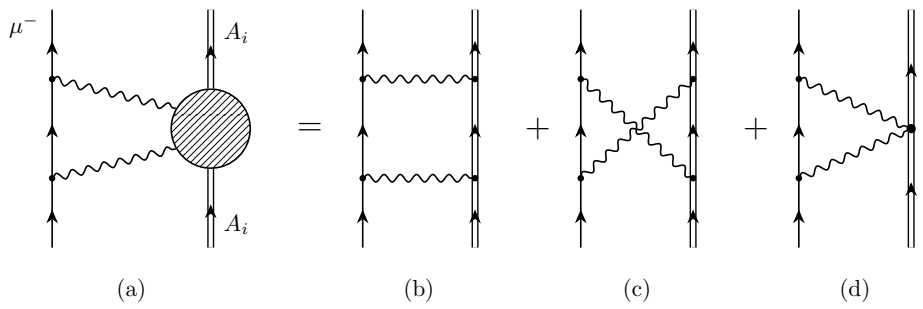

Figure 2. (**a**) Self-energy correction to the bound-muon spectrum due to nuclear polarization, given by the sum of the (**b**) ladder, (**c**) crossed, and (**d**) seagull two-photon-exchange diagrams.

Over the years, several groups have focused on the evaluation of these nuclear polarizability effects. In muonic hydrogen, one generally follows either a chiral-perturbation-theory approach, in its heavy-baryon [101–103] or manifestly covariant [104] formulation, or a data-driven approach, in which the two-photon-exchange correction is evaluated through dispersion relations using measured proton form factors and structure functions [37,38]. While the data-driven method requires subtracting an unknown function [38], effective field theories (EFTs) avoid this subtraction ambiguity altogether. Instead, EFTs introduce low-energy constants (LECs) that must be determined through matching with experimental data or the underlying fundamental theory before making predictive calculations. In muonic deuterium and heavier systems, different techniques must be applied, since one deals with very different energy scales and the most relevant physics is captured by the inter-nucleon interaction. Owing to the absence of three-nucleon forces and the simplicity of the system, works on muonic deuterium—based on pioneering analytical evaluations and potential models [105–107], chiral and pionless effective field theories [108–114], and data-driven dispersive analyses [115]—achieved remarkable precision in the determination of the nuclear structure effects, whereas in muonic tritium [22,116] and in muonic helium ions [22,116–118] the precision of the calculated $\delta_{\mathrm{NS},\mu}$ is at the level of a few percent.

Muonic helium has proven to be a particularly rich testing ground from a nuclear-structure perspective, for two reasons. The measurement of the muonic Lamb-shift in $\mu^4\mathrm{He}^+$ and $\mu^3\mathrm{He}^+$ gave the most precise extraction of the corresponding nuclear radii to date [15,16], while the comparison of the helion (^{3}He) and α-particle (^{4}He) radii confronts spectroscopy in muonic and ordinary atoms and gave rise to the helium isotope-shift puzzle—recently resolved—discussed in Section 4.5. Reducing the theoretical uncertainty on δ_{TPE} with controlled *ab initio* methods is, therefore, the key to exploiting the experimental precision and is the central theme of the remainder of this section.

4.2. Two-Photon-Exchange Amplitude in Muonic Atoms

We express the two-photon-exchange amplitude of Figure 2 as products of leptonic $L_{\mu\nu}(q,k)$, gauge $D_{\mu\nu}(q)$, and hadronic $H_{\mu\nu}(q,-q)$ tensors. The ladder (b) and crossed (c) diagrams share this factorized structure, while the seagull diagram (d) is a contact term

that does not factorize and enters through the two-photon piece $B_\perp$ of the hadronic tensor [see Equation (38)]. The amplitude reads

$$i\mathcal{M} = \int \frac{d^4q}{(2\pi)^4}\, L_{\mu\nu}(q,k)\, D^{\nu\sigma}(q)\, D^{\mu\rho}(-q)\, H_{\sigma\rho}(q,-q)\,, \tag{31}$$

where q is the four-momentum of the photon loop, and k is the muons' four-momentum.

Since muons are structureless spin-1/2 particles, the leptonic tensor, $L^s_{\mu\nu}(q,k)$, is obtained at this order in the QED expansion:

$$L^s_{\mu\nu}(q,k) = \left[-\frac{ie^2}{(k-q)^2 - m^2 + i\epsilon}\right] \bar{u}^s(k)\, \gamma_\mu \Big[(k-q)^\lambda \gamma_\lambda + m\Big] \gamma_\nu\, u^s(k)\,, \tag{32}$$

where $u^s(k)$ are the Dirac wavefunctions of the bound muon with spin s, while m denotes the muon mass and e the absolute value of its electric charge.

In both the diagrams of Figure 2 and in Equation (32), we set the spins of the incoming and outgoing muons to be equal. Spin-flip processes are generally associated with hyperfine-splitting corrections. The internal leptonic line has been evaluated using the free Dirac propagator, which yields the leading two-photon-exchange contribution to the Lamb shift, of order $(Z\alpha)^5$. Corrections to this approximation, in which the intermediate muon line is instead evaluated in the Coulomb field of the nucleus, are referred to as Coulomb-distortion effects and are of order $(Z\alpha)^6$; they are thus largely neglected in recent works. However, one Coulomb-distortion correction has been found to be logarithmically enhanced, of order $(Z\alpha)^6 \log(Z\alpha)$, and is retained in recent calculations [10,18,22,106,119]. Since the Lamb shift of muonic atoms is not sensitive to the spin-spin interaction between lepton and nucleus, one can simplify the expressions by averaging the leptonic tensor in Equation (32) over the spin.

Equation (32) has been written in the forward limit, where there is no overall momentum transfer to the muon during the two-photon process. Furthermore, one generally neglects the three-momentum of the lepton with respect to its rest mass. This approximation is motivated by the observation that light hydrogen-like atoms are loosely bound systems, where the momentum of the bound muon scales as $|\mathbf{k}| \sim m(Z\alpha)$. For light atoms, this implies $|\mathbf{k}| \ll m$. The derivations presented here are based on the applicability of this approximation, meaning that the analysis is suited to light systems where $(Z\alpha)$ is small.

The hadronic tensor satisfies crossing symmetry, $H_{\rho\sigma}(-q,q) = H_{\sigma\rho}(q,-q)$ [120]. The symmetries of the amplitude in Equation (31) can then be exploited by writing the leptonic tensor in a way that follows this symmetry as well. Adding the crossed diagram, which supplies the second time ordering with $(k+q)$ flowing through the internal line and hence the denominator $q^2 + 2mq_0$, and averaging over the muon spin, one obtains

$$L^{(S)}_{\mu\nu} = -i2\pi\alpha \left[\frac{2m\delta_{\nu0}\delta_{\mu0} - q_\mu\delta_{\nu0} - q_\nu\delta_{\mu0} + q^0 g_{\mu\nu}}{q^2 - 2mq^0 + i\epsilon} + \frac{2m\delta_{\nu0}\delta_{\mu0} + q_\mu\delta_{\nu0} + q_\nu\delta_{\mu0} - q^0 g_{\mu\nu}}{q^2 + 2mq^0 + i\epsilon}\right]. \tag{33}$$

As a next step, we specify a gauge for the photon propagators in Equation (31). Our calculation is performed in Coulomb gauge ($\nabla \cdot \mathbf{A} = 0$), which significantly simplifies the final expression for the amplitude and allows for a simpler numerical evaluation of the corrections. The photon propagator in this gauge takes the form

$$D^{\mu\nu}(q) \;=\; \begin{cases} D^{00}(q) = \dfrac{1}{\mathbf{q}^2} \\ D^{i0}(q) = D^{0j}(q) = 0 \\ D^{ij}(q) = \dfrac{1}{q^2 + i\epsilon}\left(\delta^{ij} - \dfrac{q^i q^j}{\mathbf{q}^2}\right) \end{cases}, \tag{34}$$

where Greek letters denote Lorentz indices and Roman letters denote spatial components, namely $i, j = 1, 2, 3$.

The simplifications obtained in Coulomb gauge become immediately clear when performing the contractions with the symmetrized leptonic tensor $L^{(S)}_{\mu\nu}$ of Equation (33). Many combinations vanish, and one arrives at

$$L^{(S)}_{\mu\nu}\, D^{\nu\sigma}(q)\, D^{\mu\rho}(-q) = i(4\pi\alpha)\frac{2m}{(q^2+i\epsilon)^2 - 4m^2 q_0^2}\left[\frac{\delta^\sigma_0\,\delta^\rho_0}{\mathbf{q}^2} + \frac{q_0^2}{(q^2+i\epsilon)^2}\, T^{\sigma\rho}\right], \tag{35}$$

where the free indices σ, ρ are those that contract with the hadronic tensor $H_{\sigma\rho}$. The first term in brackets carries $\sigma = \rho = 0$ and, therefore, projects onto the charge-charge response, while $T^{\sigma\rho}$ is the transverse projector, non-zero only for spatial indices $\sigma = i$, $\rho = j$,

$$T^{ij} = \delta^{ij} - \frac{q^i q^j}{\mathbf{q}^2}\,.$$

Note that this is not to be confused with the generalized Compton tensor which appears in Section 5.

4.3. The η Expansion and Multipole Sum Rules

The total amplitude follows from combining Equation (31) and (35), and the electromagnetic hadronic tensor in Equation (5), leading to

$$i\mathcal{M} = i(4\pi\alpha)^2 \int \frac{d^4q}{(2\pi)^4}\, \frac{2m}{(q^2+i\epsilon)^2 - 4m^2 q_0^2}\left[\frac{1}{\mathbf{q}^2}\, H_L + \frac{q_0^2}{(q^2+i\epsilon)^2}\, H_T\right], \tag{36}$$

where we factored out an overall $(4\pi\alpha)$ from the definition of $H_{\rho\sigma}$ and defined the longitudinal H_L and transverse H_T components of the hadronic tensor as

$$H_L \;=\; \sum_{N\neq 0} |\langle N|\rho_{\rm ch}(\mathbf{q})|0\rangle|^2 \left[\frac{1}{q_0 - \omega_N + i\epsilon} - \frac{1}{q_0 + \omega_N - i\epsilon}\right], \tag{37}$$

$$H_T \;=\; \sum_{N\neq 0} |\langle N|\mathbf{J}_\perp|0\rangle|^2 \left[\frac{1}{q_0 - \omega_N + i\epsilon} - \frac{1}{q_0 + \omega_N - i\epsilon}\right] + B_\perp(\mathbf{q})\,, \tag{38}$$

where the symbol $(\perp)$ indicates contraction with the transverse tensor T^{ij} defined after Equation (35), while $\rho_{\rm ch}(\mathbf{q}) = J_0(\mathbf{q})$ and $\omega_N = E_N - E_0$. Equations (37) and (38) follow from the spectral form of the elastic forward tensor, Equation (5), evaluated at $|i\rangle = |f\rangle = |0\rangle$, after using $E_0 - E_N \pm q_0 = \pm q_0 \mp \omega_N$. The sums are restricted to $N \neq 0$: the elastic ground-state term is independent of the nuclear excitation spectrum and is reabsorbed into the elastic (Zemach) part of the finite-size correction, so that H_L and H_T collect the genuinely inelastic, polarizability response of the nucleus.

The amplitude $i\mathcal{M}$ acts as an effective, complex muon–nucleus interaction whose real part shifts a bound-muon level $|\phi_{nL}\rangle$ by $\Delta E_{nL} = \langle\phi_{nL}|{\rm Re}(i\mathcal{M})|\phi_{nL}\rangle$. Since the muon three-momentum is neglected, this expectation value collapses to the forward amplitude weighted by $\phi^2(0) \equiv |\phi_{nL}(0)|^2$, the probability of finding the muon at the center of the nucleus. The evaluation of the amplitude is generally organized in two steps: the dominant

non-relativistic corrections are first obtained from the η expansion described in the remainder of this subsection, and the smaller relativistic corrections are subsequently added on top, as detailed below.

The non-relativistic corrections follow from the approximation ($q_0, |\mathbf{q}| \ll m$) of the integration kernels in the amplitude Equation (36). In this limit the transverse kernel carries an explicit factor q_0^2 and is, therefore, suppressed, so that the transverse response H_T vanishes identically in the leading non-relativistic term, and the whole η expansion is governed by the longitudinal (charge) response H_L [105,107,121]. The kernels are expanded in terms of the small parameter $\eta = \sqrt{2m_r\omega_N}\,|\mathbf{R}-\mathbf{R}'|$, with $\mathbf{R}, \mathbf{R}'$ being the positions of the struck protons; its expectation value scales as $\sqrt{m_r/m_p} \ll 1$, takes values $\eta \approx 0.15$ and 0.35 for $\mu^4\mathrm{He}^+$ and $\mu^3\mathrm{He}^+$, respectively [118]. Performing the q_0 and $|\mathbf{q}|$ integrations and expanding order by order in η then produces a sequence of energy-weighted multipole sum rules, which can efficiently be evaluated with the Lanczos techniques of Section 3.2; see also Ref. [84]. The leading term is the electric-dipole polarizability contribution,

$$\delta_{D1}^{(0)} = -\frac{16\pi^2}{9}(Z\alpha)^2\,\phi^2(0)\,\frac{1}{2J_0+1}\sum_{N\neq 0}\sqrt{\frac{2m_r}{\omega_N}}\,|\langle N\|\hat{D}_1\|0\rangle|^2\,, \tag{39}$$

where J_0 is the ground-state spin, and $\langle N\|\hat{D}_1\|0\rangle$ are the reduced matrix elements of the dipole operator $\hat{D}_1$, i.e., the long-wavelength limit of the $J=1$ Coulomb multipole M_{1M} of Section 2.2. Equation (39) shows that the dominant nuclear-structure correction is governed by the $\omega^{-1/2}$-weighted moment of the dipole strength, closely related to the static dipole polarizability α_D.

At sub-leading order in η, two terms appear, denoted as $\delta_{Z3}^{(1)}$ and $\delta_{R3}^{(1)}$ in Ref. [22]. The first reproduces, with opposite sign, the elastic Zemach (Friar) contribution

$$\delta_{\mathrm{Zem}} = -\frac{m_r^4}{24}(Z\alpha)^5\iint d^3R\,d^3R'\,|\mathbf{R}-\mathbf{R}'|^3\,\rho_{\mathrm{ch}}(\mathbf{R})\,\rho_{\mathrm{ch}}(\mathbf{R}')\,, \tag{40}$$

proportional to the third (Friar) moment of the charge density ρ_{ch}: in the point-nucleon limit $\delta_{Z3}^{(1)} = -\delta_{\mathrm{Zem}}$, so that the elastic piece cancels out of the total two-photon-exchange correction. Its inelastic counterpart $\delta_{R3}^{(1)}$, built on the proton-proton correlation function, enjoys no such cancellation: it vanishes for the hydrogen isotopes, which contain a single proton, but for $Z > 1$ it survives in full and is by no means small. In $\mu^3\mathrm{He}^+$, for instance, $\delta_{Z3}^{(1)}$ and $\delta_{R3}^{(1)}$ amount to $+8.3$ and -8.7 meV, respectively, each individually exceeding in magnitude the leading dipole term $\delta_{D1}^{(0)} \simeq -6.6$ meV [22]. At the following order, three further sum rules arise—an electric monopole, an electric quadrupole, and a dipole-like (D_1–D_3) (see Ref. [22] for the definition of the D_3 operator) interference response—which complete the non-relativistic η-expansion at the accuracy required for the $(Z\alpha)^5$ correction.

Two additional classes of corrections are retained at this precision. The Coulomb-distortion effect introduced in Section 4.2 generates a further electric-dipole sum rule carrying an unusual logarithmic energy weight, $\delta_C^{(0)} \propto (Z\alpha)^6\log(Z\alpha)$, which is numerically non-negligible. Secondly, relativistic corrections are added on top of the non-relativistic η expansion. They are obtained by retaining the full relativistic kinematics of the integration kernels in the amplitude Equation (36) and subtracting the leading non-relativistic contribution of Equation (39) already included above. As opposed to the non-relativistic terms which are purely longitudinal, the relativistic corrections are both longitudinal and transverse. Due to their suppression, these terms are evaluated only in the leading dipole approximation. The foundational work evaluating these non-relativistic and relativistic expansions for the nuclear polarizability in light muonic atoms was carried out in a series of studies [22,105–107,116,117,119,122,123].

4.4. Recent Ab Initio Calculations

The previous section focused on the nuclear structure corrections calculated at the level of the TPE term, namely up to order $(Z\alpha)^5$. The complete nuclear-structure correction can be schematically organized as

$$\delta_{\mathrm{NS},\mu} = \delta_{\mathrm{TPE}} + \delta_{\mathrm{3PE}} + \delta_{\mathrm{EVP}} + \delta_{\mathrm{MSEVP}} + \cdots , \tag{41}$$

where the dominant two-photon-exchange term splits into a nuclear and a single-nucleon part, $\delta_{\mathrm{TPE}} = \delta^{A}_{\mathrm{TPE}} + \delta^{N}_{\mathrm{TPE}}$, with the former computed *ab initio*; the remaining terms δ_{3PE}, δ_{EVP}, and δ_{MSEVP} are the three-photon-exchange [123], the electron vacuum-polarization, and the muon self-energy and vacuum-polarization corrections [10], respectively.

Modern calculations evaluate the nuclear part $\delta^{A}_{\mathrm{TPE}}$ from the sum rules of Section 4.3 with the many-body machinery of Section 3. The ground state $|0\rangle$ follows from a χEFT Hamiltonian solved with the effective-interaction hyperspherical-harmonics (EIHH) method, which reaches sub-percent accuracy for the three- and four-body nuclei [18,22,59], while the energy-weighted response is obtained with the Lanczos-based methods of Section 3.2, bypassing the explicit construction of the excited states $|N\rangle$—the same response machinery later applied to the γW-box amplitude in Section 5. The χEFT truncation error is propagated through the Bayesian analysis of Section 3.3 [Equation (28)]. Applied to muonic atoms, this replaces the earlier practice of estimating the uncertainty by comparing a χEFT prediction with a phenomenological potential, placing the error bars on a firm statistical footing [18,99,118].

State-of-the-art results at N^{3}LO for muonic helium are summarized in Table 1. They give $\delta^{A}_{\mathrm{TPE}} = -14.868(364)$ meV in $\mu^3\mathrm{He}^+$ and $-8.751(322)$ meV in $\mu^4\mathrm{He}^+$ [18], to be compared with the previous values $-14.72(31)$ and $-8.49(39)$ meV [22,117]. The Bayesian analysis increases the $\mu^3\mathrm{He}^+$ uncertainty by 17% and reduces the $\mu^4\mathrm{He}^+$ one by 17%, placing both on a common statistical basis. The associated dipole polarizabilities, $\alpha_{\mathrm{D}} = 3.514(68)$ and $1.909(96)$ fm^3 for ^{3}He and ^{4}He, agree with earlier determinations [122]. Combined with the remaining terms of Equation (41) taken from [10] and the measured Lamb shifts [15,16], these corrections yield the charge radii listed in Table 1. Note that these calculations do not include two-body current effects. For the muonic Lamb shift, however, such contributions are heavily suppressed in χEFT because the shift is dominated by the longitudinal hadronic tensor, and two-body charge operators enter only at higher chiral orders [39].

Table 1. Nuclear-structure corrections in muonic helium at N^{3}LO and the extracted charge radii, from Ref. [18]. Uncertainties are obtained from a Bayesian analysis of the χEFT truncation.

	$\delta^{A}_{\mathrm{TPE}}$ (meV)	$\delta_{\mathrm{NS},\mu}$ (meV)	r_c (fm)
^{3}He	$-14.868(364)$	$-15.644(427)$	$1.9704(11)$
^{4}He	$-8.751(322)$	$-9.541(368)$	$1.6793(10)$

4.5. Impact on the Helium Isotope-Shift Puzzle

A particularly sensitive observable is the difference of the squared charge radii of the two helium isotopes, $\delta r^2 = r_c^2(^3\mathrm{He}) - r_c^2(^4\mathrm{He})$. Because the dominant theoretical uncertainties are strongly correlated between ^{3}He and ^{4}He, δr^2 can be determined more precisely than either radius individually [18]. It is moreover accessible by two independent routes; from the absolute radii measured in muonic helium through the Lamb shift, and from the isotope shift of the $2\,^3S \to 2\,^1S$ transition in electronic helium.

Using the muonic-helium nuclear-structure corrections of Section 4.4, the muonic route gives $\delta r^2|_{\mu} = 1.0626(29)$ fm^2 [18], a 6% improvement of the uncertainty over the value $1.0636(6)_{\mathrm{expt}}(30)_{\mathrm{theo}}$ fm^2 extracted directly from the CREMA measurements [16],

while the ordinary-atom route gives $\delta r^2|_e = 1.0758(15)$ fm^2 [18], basically matching the value 1.0757(15) fm^2 of Ref. [17] obtained using the previous theoretical calculation for the nuclear structure effects. At the time of the analysis of Ref. [18], the two routes disagreed at the 4σ level; far from resolving the tension, the improved nuclear-structure input increased the earlier 3.6σ discrepancy [16]. Crucially, the Bayesian framework showed that the shift needed to reconcile the two routes was excluded on the nuclear-structure side at the 95% confidence level [18], exonerating the nuclear corrections and pointing instead to experimental systematics or neglected atomic-theory contributions.

The resolution came from the atomic theory of ordinary helium. Qi and collaborators [19] identified a previously neglected hyperfine mixing of the $2\,^1S$ and $2\,^3S$ levels of ^{3}He with higher S states ($n > 2$), which shifts the $2\,^3S \to 2\,^1S$ isotope shift and lowers the ordinary-atom value to $\delta r^2|_e = 1.0693(15)$ fm^2, reducing the tension with respect to Ref. [16] to 1.7σ. Pachucki and collaborators subsequently derived the complete second-order hyperfine correction [20], obtaining $\delta r^2|_e = 1.0678(7)$ fm^2, which agrees with the muonic value of Ref. [16] at the 1.3σ level and with the improved determination of Ref. [18] at 1.7σ. The resulting consistency of the two routes validates the extraction of absolute charge radii from muonic atoms and supports its extension to the heavier systems.

4.6. Heavy Muonic Atoms and Highly Charged Ions

While the *ab initio* methods combined with χEFT discussed above provide rigorous uncertainty quantification for the lightest nuclei ($A \leq 4$), they are not feasible for the heavy systems probed by muonic X-ray spectroscopy—which accesses nuclear charge radii through the energies of the $np \to 1s$ transitions emitted during the muonic-atom cascade, and has recently experienced a strong revival. On the experimental side, the QUARTET collaboration at the Paul Scherrer Institute aims at measuring the absolute charge radii of light nuclei ($3 \leq Z \leq 10$, from lithium to neon) with up to an order-of-magnitude improved accuracy by detecting the low-energy muonic X-rays with metallic magnetic calorimeters [33,34]. In parallel, the muX project has developed a repeated muon-transfer technique in a high-pressure hydrogen–deuterium gas cell that enables muonic-atom spectroscopy with microgram amounts of target material, giving access to rare and radioactive species such as ^{226}Ra and ^{248}Cm [124,125]. This program has recently been extended to the medium-mass region, where a high-statistics measurement of muonic ^{35,37}Cl with a large-scale germanium detector array determined the charge radii of the stable chlorine isotopes with an order-of-magnitude improvement in precision [35]. The chlorine measurement was accompanied by a dedicated theory framework for medium-mass muonic atoms [126]. Across this entire program, the nuclear polarizability correction remains the most challenging and uncertain theoretical input, and its evaluation has consequently attracted renewed attention [126–130].

This scrutiny is driven by a long-standing puzzle: the $nP_{1/2}$–$nP_{3/2}$ fine-structure splittings measured in heavy muonic atoms such as μ-^{90}Zr, μ-^{120}Sn and μ-^{208}Pb show persistent anomalies between theory and experiment that have traditionally been ascribed to the nuclear polarizabilities [129]. Because an *ab initio* description of heavy nuclear spectra is out of reach, the nuclear excitation spectrum entering the correction is instead computed within the random-phase approximation (RPA) on top of a self-consistent Hartree–Fock mean field built from an effective Skyrme interaction [129]. The muon-nucleus interaction is treated in a fully field-theoretical framework; the same ladder, crossed and seagull diagrams of Figure 2 reappear [129,130].

A systematic study across nine Skyrme parametrizations indicated that the resulting nuclear-model uncertainty on the nuclear polarizability correction is much smaller than the persistent theory–experiment discrepancies, suggesting that the nuclear polarizability is not

the origin of the fine-structure anomalies, which must instead be sought in refined QED or recoil corrections [129]. This conclusion has recently been substantiated: a re-evaluation of muonic ^{208}Pb combining state-of-the-art QED with modern nuclear polarizability models closed the long-standing fine-structure-anomaly gap [131], while an all-order treatment of the relativistic-recoil effect resolved the analogous puzzle in muonic ^{90}Zr [132].

5. Recent Progress in Superallowed Nuclear Beta Decays

Precision beta decay provides one of the cleanest low-energy probes of the weak-charged-current interaction [4,133,134]. Nuclear Fermi transitions, a special type of weak transition in nuclei, are decays of the kind $(J^\pi, T) = (0^+, 1) \to (0^+, 1)$ for which the leading amplitude is heavily constrained by the spin-isospin symmetries of the external states. These transitions give clean access to the Cabibbo–Kobayashi–Maskawa (CKM) up–down-quark-mixing element V_{ud} and, hence, to the top-row unitarity test of the SM. At the quark level, the weakly charged current is given by the Lagrangian

$$\mathcal{L}_{\mathrm{WCC}} = -\frac{g}{2\sqrt{2}} \begin{pmatrix} \bar{u}_L & \bar{c}_L & \bar{t}_L \end{pmatrix} \gamma^\mu W^+_\mu V_{\mathrm{CKM}} \begin{pmatrix} d_L \\ s_L \\ b_L \end{pmatrix} + \text{h.c.}, \tag{42}$$

where $e = g \sin(\theta_{\mathrm{W}})$ defines the weak coupling constant, and the CKM matrix enters as a 3×3 unitary matrix in flavor space [135,136] with the top-row unitarity condition

$$|V_{ud}|^2 + |V_{us}|^2 + |V_{ub}|^2 = 1. \tag{43}$$

At the precision of $\mathcal{O}(10^{-4})$ required for modern tests of CKM matrix unitarity, the tree-level amplitude is not sufficient, and electroweak radiative corrections (EWRC) must be explicitly included in the extraction of V_{ud}; a relevant process is the γW box, whose basic physics is illustrated in Figure 3. The evaluation of such radiative corrections in nuclear theory has become the defining challenge in precision extractions of V_{ud}. A general current-algebra framework developed some time ago by A. Sirlin [137] forms the basis of the analysis presented in the subsequent sections.

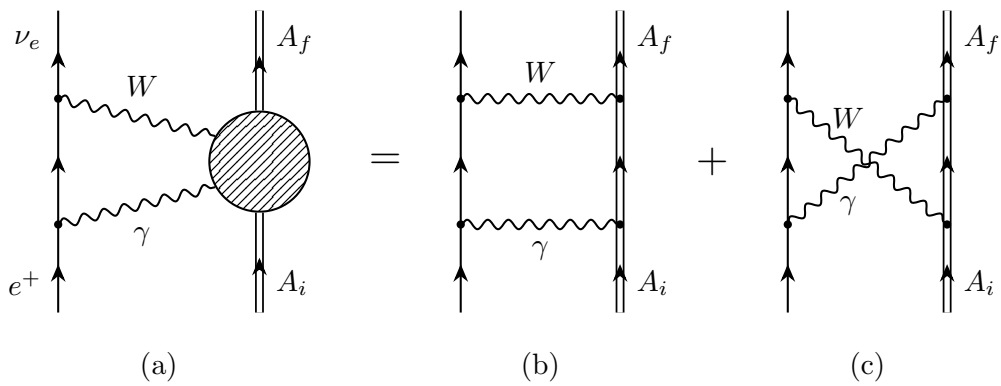

Figure 3. Pictured is the contribution from a higher-order, virtual electroweak box diagram to the beta decay process of $\Psi_i \to \Psi_f + \nu_e + e^+$, known as the γW box.

We will assume isospin symmetry in the following relativistic derivations; however, it should be noted that isospin-breaking effects are included in all nuclear-structure-dependent pieces of the calculation. This is well-enough justified as superallowed transitions occur between nearly-degenerate isospin analog states. Further, note that the discussion is tailored towards nuclear decays.

5.1. Extraction of V_{ud} from Superallowed Decays

For a given nuclear Fermi transition, $\Psi_i(p) \longrightarrow \Psi_f(p') + e^+(p_e) + \nu_e(p_\nu)$, the tree-level amplitude between relativistic lepton-nucleus, plane-wave states is

$$iM_0(p_f, p_i, k_f, k_i) = -i\frac{G_F V_{ud}^*}{\sqrt{2}}\, L_\lambda(k_f, k_i)\, F^\lambda(p_f, p_i), \tag{44}$$

where $F^\lambda(p', p)$ is the amplitude of the charged-weak current with external $J^\pi = 0^+$ and $T = 1$ nuclear states, L_λ is the leptonic amplitude, and $G_F/\sqrt{2} = g^2/8M_W^2$ is the Fermi constant. They are, respectively, given by

$$F^\lambda(p_f, p_i) = \langle f; \mathbf{p}_f | J_W^{\dagger\lambda}(q) | i; \mathbf{p}_i \rangle = f_+(t)\,(p_f + p_i)^\lambda + f_-(t)\,(p_f - p_i)^\lambda,$$

$$L^\lambda = \bar{u}_e \gamma^\lambda (1 - \gamma_5) v_\nu,$$

with $t = (p_f - p_i)^2$, and the former is written in the isospin-symmetric limit with spinless external states (exact for superallowed transitions). These form factors are normalized, such that $f_+(0) = \sqrt{2}$ and $f_-(0) = 0$ in $T = 1$ systems. At the leading order in $|\mathbf{p}|/m$, the axial-vector piece of the current does not contribute, and the conserved-vector-current hypothesis implies that the vector matrix element is fixed by isospin symmetry to be $M_{F0} = \sqrt{2}$.

Then, for superallowed transitions, one may write down the differential rate in the point-like nucleus limit as

$$d\Gamma = dE_e\, \frac{G_F^2\, g_v^2\, m_e^5\, |M_{F0}|^2 |V_{ud}|^2}{2\pi^3}\, \frac{1}{m_e^5}\, |\vec{p}_e|\, E_e\, (E_0 - E_e)^2\, F(Z_f, E_e), \tag{45}$$

where $F(Z, E_e)$ is the Fermi function [138–140]. Many corrections arise in this expression as non-point-like distributions and higher-order processes for the nucleus are considered; e.g., see Section 3.1 of Ref. [5] for a summary. After integration over the positron phase space to produce the dimensional statistical phase-space factor f and multiplication by the half-life of the decay process $t = \ln 2/\Gamma$, we have

$$|V_{ud}|^2 = \frac{K}{G_F^2\, g_v^2\, |M_{F0}|^2 f t} + \text{higher-order corrections}, \tag{46}$$

where K is a transition-independent constant. The promise of these decays is simple: any measurement of a single or set of the available superallowed transitions should lead to a consistent extraction of V_{ud}. However, this is hardly the case at the current precision level due to the aforementioned requirement of corrections to the decay rate.

As shown by Sirlin, use of the conserved-vector-current hypothesis and electromagnetic Ward identities allows one to express the combination of vertex corrections and radiative diagrams at $\mathcal{O}(G_F\,\alpha)$ into a set of structure-independent universal logarithms, a long-distance outer correction, and a hadronic-structure-sensitive inner correction. Schematically, the correction to the amplitude is then given in terms $\mathcal{M}_0$ as

$$\delta\mathcal{M} = \mathcal{M}_0\, \frac{\alpha}{2\pi}[\text{universal logs} + \delta_{\text{outer}} + \delta_{\text{inner}}] + \mathcal{O}(G_F\,\alpha^2). \tag{47}$$

The dominant part of the outer correction δ_R' accounts for infrared QED effects, e.g., bremsstrahlung photon emission, as well as Coulomb distortion of the positron wave function [141–145]; typically quoted to order $Z\alpha^3$, the outer correction has seen

increased scrutiny in recent years which call into question certain results from historical works [139,140,146,147]. The short-range analogue known as the inner correction Δ_R^V is universal to all superallowed transitions and comprises several effects, the most challenging of which to compute is the hadronic-structure-dependent γW box which dominates the uncertainty; theoretical errors were greatly improved in the last eight years [6,148–151] and led directly to the observed tension with unitarity. In addition to the QED and intra-nucleon-structure effects, β decay in composite hadrons like nuclei begets additional structure corrections, namely, $\delta_{\rm C}$ and $\delta_{\rm NS}$. The former is known as the isospin symmetry breaking correction and it parameterizes the renormalization of the Fermi amplitude due to isospin-non-conserving interactions, i.e., the strong and Coulomb interactions. The latter parameterizes the modification of the free-nucleon γW box due to the nuclear medium, and one may approximately separate the nucleon- and nuclear-level effects as

$$1+\delta_{\rm inner} = 1+\Delta_R^U + 2\Box_{\gamma W}^n + 2(\mathrm{Re}\,\Box_{\gamma W}^{\rm nuc.} - \Box_{\gamma W}^n) \approx (1+\Delta_R^V)(1+\delta_{\rm NS}), \tag{48}$$

where Δ_R^U (and consequently Δ_R^V) is a piece universal to all superallowed decays, $\Box_{\gamma W}^n$ is the free-nucleon box contribution, and $\Box_{\gamma W}^{\rm nuc.}$ is the nuclear box contribution in a given transition [5]. After the appropriate SM corrections are applied, we have

$$|V_{ud}|^2 = \frac{K}{G_F^2\, g_v^2\, |M_{F0}|^2 \mathcal{F}t\,(1+\Delta_R^V)} \qquad \mathcal{F}t = ft(1+\delta_R')(1-\delta_{\rm C}+\delta_{\rm NS}), \tag{49}$$

and different nuclei should yield a common corrected $\mathcal{F}t$ value to the present desired precision level, and hence a consistent value of V_{ud}.

This is precisely the comparison shown on the right-hand side of Figure 4, with the sub-figures taken from Ref. [4]. The issue is severe as the uncorrected ft values, shown in the upper plot (a), are not transition-independent at the required precision level. This is in contrast to the corrected $\mathcal{F}t$ values, shown in the lower plot (b), which encode the electroweak radiative, recoil, and nuclear-structure corrections. Clearly, the $\mathcal{O}(10^{-4})$ effects do much to restore the expected transition-independent behavior. Historically speaking, the only approach to successfully produce a quasi-alignment of the nucleus-independent $\mathcal{F}t$ values across the chart is that shown in Figure 4, and it is based upon shell-model-type calculations with Woods–Saxon potentials (see Ref. [4] for the latest review and references therein). Alternative approaches in the literature have not been able to produce the same agreement obtained by Hardy and Towner, for example, Refs. [152,153]. Notwithstanding early efforts on the front of $\delta_{\rm C}$ [154,155] and prior to the last few years, in the last two decades, the *ab initio* nuclear theory community has not pushed hard to reduce the theoretical uncertainties despite some criticism of their estimates [156–158].

Herein, we are primarily concerned with the γW box process, which gives rise to both Δ_R^V and $\delta_{\rm NS}$. The present unitarity test, and any purported claim of beyond SM physics in superallowed decays, is sensitive to such electroweak effects at the $\mathcal{O}(10^{-4})$ level. Modern analyses report a two-to-three-sigma tension between CKM unitarity and experiments [6,24,32,148,159,160], as shown in the up-to-date plot of the quoted PDG 2024 values for $|V_{ud}|$ and $|V_{us}|$ on the left-hand-side of Figure 4. Importantly, from Ref. [23] to Ref. [4], the overall uncertainty inflated by a factor of 2× after recognition that the reported nuclear-structure uncertainties were far less under control than previously thought. The ad hoc modeling of the quasi-elastic nuclear response to the external probes via Fermi gas theory elucidated the unknown sensitivity to the nuclear spectrum. As a result, $\delta_{\rm NS}$ became the dominant part of the uncertainty budget to V_{ud}

extraction [5,161], making its evaluation from *ab initio* theory a priority of the nuclear theory community [162].

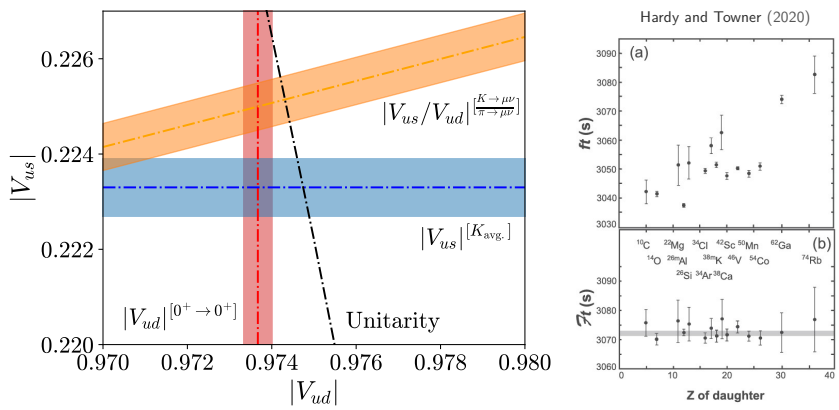

Figure 4. (**Left**) The modern CKM unitarity landscape with values for V_{ud}, V_{us} and the ratio V_{ud}/V_{us} annotated with their corresponding experimental extractions [7]. The dash-dot lines and bands, respectively, represent the central value and uncertainty in the extraction of a given top-row element of the CKM matrix. The black line indicates the exact unitarity constraint. Note that the contribution of V_{ub} is $\mathcal{O}(10^{-5})$ and is thus negligible at this precision. (**Right**) Figures taken directly from Ref. [4] with evaluations for a range of nuclei from ^{10}C to ^{74}Rb of (**a**) ft values, as extracted from the experiment; (**b**) corrected $\mathcal{F}t$ values with higher-order SM processes included.

5.2. The γW Box Nuclear-Structure-Dependent Radiative Correction

Thus came a flurry of works on the nuclear-structure-dependent corrections to superallowed decays; see Refs. [134,163] for a survey of the status of modern theory and experiment. For $\delta_{\rm NS}$, a more rigorous calculation within the current algebra formalism managed to improve the uncertainty in the ^{10}C $\to$ ^{10}B by a factor of 1.6$\times$ [31], while a novel effective field theory (EFT) approach that dramatically simplifies the nuclear many-body calculation was implemented for the ^{10}C $\to$ ^{10}B [164] and ^{14}O $\to$ ^{14}N [165,166] decays, albeit with a dependence on two new low-energy constants for beta decay. Moreover, a third way based on the manifestly covariant construction of current-current correlators in point-like effective theory has been developed [167,168], which systematically organizes all corrections at one loop and beyond, and may thus be mechanically advantageous over the traditional formalism; such a theory may also be incorporated as an additional step in the tower of EFTs applied in Refs. [164–166]. Furthermore, a new perturbative approach has been proposed for the isospin-symmetry-breaking correction [169], while an independent attempt at extracting $\delta_{\rm C}$ from the Fermi matrix element in Quantum Monte Carlo saw strong dependence on the nuclear Hamiltonian [170]. While tremendous progress has been made, these works are not the definitive statement on superallowed decays, and there is much to be done in the coming years. We now discuss the current algebra formalism utilized in Ref. [31], which presently provides the most precise determination of $\delta_{\rm NS}$ in the ^{10}C $\to$ ^{10}B transition.

Applying Sirlin's representation [133,137] to study the one-loop radiative corrections to hadronic decays yields a number of diagrams at $\mathcal{O}(G_F\,\alpha)$, the most important of which we have identified in the previous section to be the γW box diagram. This correction is the only one which truly probes the non-perturbative structure of the external hadronic states. The correction to the amplitude may be split as $\delta\mathcal{M}_{\gamma W} = \delta\mathcal{M}^a_{\gamma W} + \delta\mathcal{M}^b_{\gamma W}$ with the first term in partial cancellation with the hadronic vertex correction, leaving a residual integral negligible in the Fermi amplitude when taken in the forward limit. $\delta\mathcal{M}^b_{\gamma W}$ is then the only piece of the γW diagram which remains to be evaluated (see Equation (30) of Ref. [133]) and it is given by

$$\delta\mathcal{M}^{b}_{\gamma W} = -i\frac{e^2}{\sqrt{2}}G_F\, L_\lambda \int \frac{d^4q}{(2\pi)^4}\,\frac{M_W^2}{M_W^2-q^2}\,\frac{1}{q^2+i\epsilon_2}\,\frac{\epsilon^{\mu\nu\alpha\lambda}q_\alpha}{(p_e-q)^2-m_e^2+i\epsilon_1}\,T_{\mu\nu}, \tag{50}$$

where the nuclear-structure-dependent piece is the generalized Compton tensor $T_{\mu\nu}$. Its operator content is that of the generalized hadronic tensor in Equation (2), with one electromagnetic and one charged-weak current, and whose spectral representation is given in Equation (6). Note that, following the conventions in the β-decay literature [133,137,161], the Compton tensor $T_{\mu\nu}$ is defined with relativistically normalized external nuclear states, i.e., $\langle f;\mathbf{p}_f|i;\mathbf{p}_i\rangle = 2E_{\mathbf{p}_i}\,(2\pi)^3\,\delta^{(3)}(\mathbf{p}_f-\mathbf{p}_i)$, in contrast to the unit-normalized, non-relativistic states used throughout Section 2. The leading-order matching between the non-relativistic and relativistic amplitudes is given below.

First, via separation of the weak current as $J_W = J_V - J_A$, we may further decompose this contribution into vector and axial-vector pieces, such that

$$\mathcal{M}^{b}_{\gamma W} = \mathcal{M}^{b,VV}_{\gamma W} + \mathcal{M}^{b,VA}_{\gamma W}, \tag{51}$$

for which the vector–vector piece vanishes in the forward limit and for exact isospin symmetry since $T^{\mu\nu}$ only depends on two external momenta; the only Lorentz covariant structures that can be built are $g_{\mu\nu}$, $p_\mu p_\nu$, $p_\mu q_\nu$, $p_\nu q_\mu$, and $q_\mu q_\nu$, all of which vanish under contraction with $\epsilon^{\mu\nu\alpha\lambda}q_\alpha$. Then, under this set of approximations, all that remains is the vector–axial–vector contribution, which can be shown to factorize as

$$i\mathcal{M}^{b,VA}_{\gamma W} = i\mathcal{M}_0 \times \langle\, \mathrm{Re}\,\Box^{b}_{\gamma W}(E_e)\,\rangle, \tag{52}$$

where $\mathcal{M}_0$ is the tree-level amplitude, and $\langle\, \mathrm{Re}\,\Box^{b,\mathrm{nuc.}}_{\gamma W}(E_e)\,\rangle$ is the result of averaging the real part of the nuclear γW box function over the positron phase space. In the isospin-symmetric forward limit, with $M_i = M_f = M$ and $p_i = p_f = p = (M,\mathbf{0})$, the contribution of the vector–axial–vector γW box may be written as [161]

$$\begin{aligned}\Box^{b}_{\gamma W}(E_e) = e^2 \int \frac{d^4q}{(2\pi)^4}\,\frac{M_W^2}{M_W^2-q^2}\,\frac{1}{q^2+i\varepsilon_1}\,\frac{1}{(p_e-q)^2-m_e^2+i\varepsilon_2}\\ \times\,\frac{|\mathbf{q}|\big(|\mathbf{q}|-\nu\beta^{-1}x\big)}{\nu}\,\frac{T_3(\nu,\mathbf{q})}{Mf_+},\end{aligned} \tag{53}$$

where $p_e = (E_e,\mathbf{p}_e)$ is the positron momentum, $q = (\nu,\mathbf{q})$ is the virtual gauge boson loop momentum, $x = \hat{\mathbf{p}}_e\cdot\hat{\mathbf{q}}$ is the angle between the positron and emitted boson, and $\beta = |\mathbf{p}_e|/E_e$ the positron velocity. The weak-boson propagator has been left in the integrand for completeness, although the relevant nuclear response is concentrated at momentum scales far below M_W. All nuclear structure information is contained in the spin-invariant, parity-odd amplitude T_3 that appears in Equation (53). For spin-zero external states, this is the only surviving piece of the Compton tensor and, therefore, the only relevant part of the hadronic tensor for the γW box correction; a complete expression in terms of the multipole expanded currents is provided in the following section. It is conventionally defined as [161]

$$T^{\mu\nu}\big|_{\mathrm{VA}} = \frac{i\epsilon^{\mu\nu\alpha\beta}p_\alpha q_\beta}{2p\cdot q}\,T_3, \tag{54}$$

where the factor of $2p\cdot q$ is a convention and is not to be confused with the normalization of the tensor itself. We note the convention $\epsilon^{0123} = -1$ in the above expression.

We now comment on the contact term $B^{\mu\nu}_{\mathrm{em\,W}}(\mathbf{q})$ in the non-relativistic hadronic tensor. This term arises from physical states at scales not described by the low-energy effective

theory, e.g., multi-hadron intermediate states or nuclear shadowing effects, and these states are, therefore, not explicitly present in the spectral decomposition of the hadronic tensor in Equation (6). Now, we are only interested in the anti-symmetric part of the Compton tensor T_3 and so, when contracted with the Levi–Civita in Equation (54), the term in the photon propagator with the gauge fixing parameter, which goes as $\sim(1-\xi)\, q_\mu q_\nu$ vanishes. Unlike in two-photon exchange where a seagull vertex is present to guarantee gauge invariance of the hadronic tensor (represented in Coulomb gauge), the gauge fixing parameter is irrelevant and the result is manifestly gauge invariant. The contributions which appear in $B^{\mu\nu}_{\mathrm{em\,W}}(\mathbf{q})$ are not needed to regulate any divergences but are associated with physics with quark-gluon degrees of freedom, for example, the free-neutron γW box function.

While $T^{\mu\nu}$ is built from relativistically normalized states, one needs to match onto the amplitudes in non-relativistic nuclear many-body theory, i.e., to match onto the unit-normalized tensor in Equation (6). At leading order in the heavy-particle limit, the amplitude-level matching between the two descriptions amounts to an overall normalization of the external states as

$$\bar{u}_f(\mathbf{p}_f)\,\Gamma_O\, u_i(\mathbf{p}_i) = \sqrt{4M_f M_i}\,\langle f|\int d^3x\, O(x)\,|i\rangle + \cdots\,, \tag{55}$$

where $\mathcal{O}(x)$ is a given current operator with Dirac matrix representation Γ_O, and the ellipses denote relativistic corrections of $\mathcal{O}(\langle \mathbf{p}^2\rangle/M)$ to the amplitude (see Section XII–1 of Ref. [171] for a comprehensive discussion). Applying Equation (55) to the Compton tensor gives $T^{\mu\nu} = i/2\sqrt{4M_f M_i}\; H^{\mu\nu}_{\mathrm{em\,W}} + \cdots$ where the normalization of the intermediate spectrum cancels against the relativistic completeness measure. The relativistic amplitude T_3 entering the γW box can, therefore, be evaluated entirely with unit-normalized eigenstates of the non-relativistic nuclear Hamiltonian.

Thus, the task is to compute T_3 with sufficient nuclear-structure input and to insert it into the loop integral defining the γW box function, after which one averages over the positron phase space to obtain

$$\Box^{b,\mathrm{nuc.}}_{\gamma W} = \langle\, \mathrm{Re}\,\Box^{b,\mathrm{nuc.}}_{\gamma W}(E_e)\,\rangle = \frac{\int_{m_e}^{E_0} dE_e\, |\vec{p}_e|\, E_e(E_0-E_e)^2\, F(Z_f,E_e)\,\mathrm{Re}\,\Box^{b,\mathrm{nuc.}}_{\gamma W}(E_e)}{\int_{m_e}^{E_0} dE_e\, |\vec{p}_e|\, E_e(E_0-E_e)^2\, F(Z_f,E_e)}. \tag{56}$$

When properly combined with the state-of-the-art result for free neutron decay [6], this provides the nuclear-structure-dependent electroweak radiative correction

$$\delta_{\mathrm{NS}} = 2(\Box^{b,\mathrm{nuc.}}_{\gamma W} - \Box^{n}_{\gamma W}), \tag{57}$$

to a given Fermi transition.

5.3. The Forward Hadronic Tensor and the γW Box Loop Integral

The nuclear amplitude T_3 is evaluated by expanding the electroweak currents in Coulomb, longitudinal, transverse electric, and transverse magnetic multipoles (see the discussion in Section 2.2). The expanded form is given by

$$\begin{aligned} T_3(\nu,\mathbf{q}) = 4\pi i\,\frac{\nu}{|\mathbf{q}|}\sqrt{M_i M_f}\sum_{J=1}^{\infty}(2J+1) \\ \times\Big[\,\langle f|\left\{T^{\mathrm{el}}_{\mathrm{em},J0}(z_f-H)^{-1}T^{5,\mathrm{mag}}_{\mathrm{W},J0} - iT^{\mathrm{mag}}_{\mathrm{em},J0}(z_f-H)^{-1}iT^{5,\mathrm{el}}_{\mathrm{W},J0}\right\}|i\rangle \\ +\langle f|\left\{T^{5,\mathrm{mag}}_{\mathrm{W},J0}(z_i-H)^{-1}T^{\mathrm{el}}_{\mathrm{em},J0} - iT^{5,\mathrm{el}}_{\mathrm{W},J0}(z_i-H)^{-1}iT^{\mathrm{mag}}_{\mathrm{em},J0}\right\}|i\rangle\,\Big], \end{aligned} \tag{58}$$

where the label "5" denotes a multipole arising from the axial-vector part of the weak-charged current, the arguments of the resolvents contain $z_i = M_i - \nu + i\varepsilon_3$ and $z_f = M_f + \nu + i\varepsilon_3$, and we have further made use of Equation (55) to convert the amplitude into its non-relativistic form. The amplitudes of the resolvent are handled in full by use of the Lanczos methods described in Section 3.2. In pragmatic calculations, the sum over multipoles is truncated at some finite J to reach the desired precision.

The loop integral in Equation (53) contains poles from the photon propagator, the electron propagator, and the nuclear propagators in T_3, so direct principal value integration over real ν is inconvenient. As in Ref. [31], one may deform the ν contour to the imaginary axis, $\nu = i\nu_E$, while accounting for any poles enclosed by the contour deformation. Tracking the various poles in Figure 5 then gives

$$\Box^b_{\gamma W} = \left(\Box^b_{\gamma W}\right)^{\uparrow}_{\text{Wick}} + \left(\Box^b_{\gamma W}\right)_{\text{Res},T_3} + \left(\Box^b_{\gamma W}\right)_{\text{Res},e}. \tag{59}$$

The first term is the Wick-rotated integral with the direction of integration upwards along the $\text{Im}\,\nu$ axis. The second term collects residues of the Compton amplitude located in quadrant III, which arise from low-lying states in the intermediate spectrum below the final state 0^+ [31], with

$$\nu_n = \Delta_n + \frac{|\mathbf{q}|^2}{2M_n} - i\varepsilon \qquad \Delta_n = M_n - M_f < 0.$$

The Compton residue contribution is incurred only on the momentum interval

$$|\mathbf{q}| \leq \sqrt{-2\Delta_n M_n}, \tag{60}$$

after which the pole escapes the contour. The third term is generated by the electron propagator poles enclosed by the contour in quadrant I; we neglect to discuss this contribution further since it has been shown to be negligible by several orders of magnitude. Contributions from the large semicircles vanish in a given non-relativistic nuclear model, and the pole associated with the W propagator lies at momenta of order M_W, well outside the support of a non-relativistic calculation.

The Wick term has the generic form

$$\left(\Box^b_{\gamma W}\right)_{\text{Wick}}(E_e) = e^2 \int_0^\infty d|\mathbf{q}| \int_{-\infty}^{\infty} d\nu_E\, K(i\nu_E, |\mathbf{q}|; E_e)\, \frac{i\, T_3(i\nu_E, \mathbf{q})}{M f_+}, \tag{61}$$

and the Compton residue term

$$\left(\Box^b_{\gamma W}\right)_{\text{Res,T3}}(E_e) = e^2 \int_0^\infty d|\mathbf{q}|\; K(\nu_k, |\mathbf{q}|; E_e)\, \frac{i\,\text{Res}\, T_3(\nu_k, \mathbf{q})}{M f_+}, \tag{62}$$

where the function K contains the photon, electron, and W-boson propagators with the angular integration in Equation (53) having been performed analytically. The appearance of K in the Wick contribution is understood as the analytic continuation of the function K as it would appear in Equation (53). The decomposition in Equation (59) then provides a controlled way of computing $\Box^b_{\gamma W}(E_e)$ on the real-ν axis.

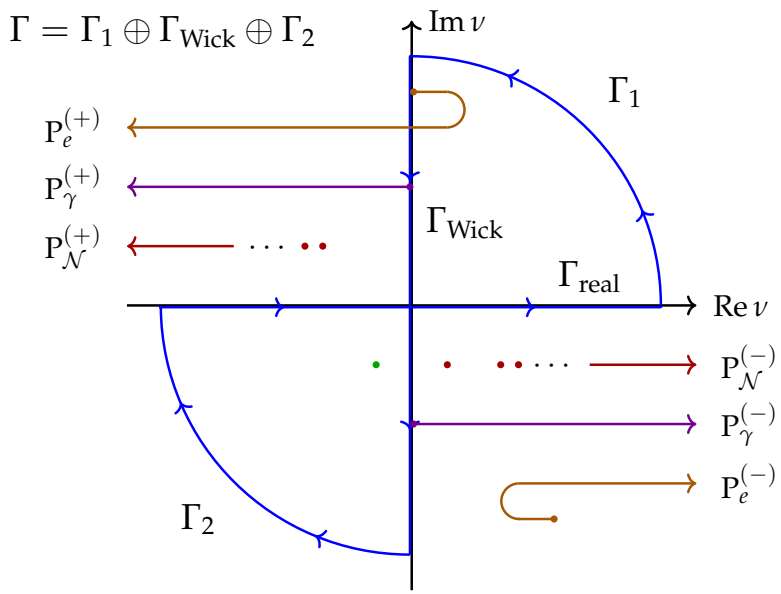

Figure 5. Example trajectories of the ν-integral poles in Equation (53) arising from the dynamics of: (i) the nuclear propagators in T_3, plotted in red for $\Delta_n > 0$ and green for $\Delta_n < 0$; (ii) the photon propagator, plotted in purple; and (iii) the electron propagator, plotted in orange. The corresponding sets are labeled by $\mathcal{N}$, γ and e, respectively. The chosen contour deformation Γ is the oriented contour defined by $\Gamma = \Gamma_1 \oplus \Gamma_{\text{Wick}} \oplus \Gamma_2$, shown in blue.

5.4. Ab Initio Calculations in Light Nuclei and Impact on CKM Unitarity

In Table 2, we summarize the state-of-the-art results for the electroweak radiative corrections to the $^{10}\text{C} \to {}^{10}\text{B}$ transition with δ_{NS} as computed in the current algebra (CA) formalism, along with its closest analog in the EFT formalism, $\delta_{\text{NS}}^{(0)}|_{\text{mag+LS}}$, which only includes the long-range part of the EFT calculation (and thus the shown uncertainties are not representative of the complete result). We further note that, while there is significant overlap in the physics of these two quantities, they are not directly comparable, and there is an ongoing effort to perform rigorous matching between the two formalisms (private communication from C.-Y. Seng). Most important to observe is that the modern results are discrepant with the values adopted in the Hardy and Towner 2014 critical survey on superallowed decays [23]. The observed shift confirms that an *ab initio* treatment of the nuclear response with genuine many-body approaches provides a numerical enhancement to prior estimates of the same physics.

Table 2. A summary of state-of-the-art results for evaluations of δ_{NS} in the current algebra (CA) formalism and the long-range part of the radiative correction $\delta_{\text{NS}}^{(0)}|_{\text{mag+LS}}$ in the EFT formalism for the $^{10}\text{C} \to {}^{10}\text{B}$, as compared to the last two available surveys on superallowed decays from Hardy and Towner. The results are quoted in the table as provided in their corresponding references.

[%]	$^{10}\text{C} \to {}^{10}\text{B}$
CA δ_{NS}	$-0.422(29)_{\text{nuc}}(12)_{n,\text{el}}$ [31]
EFT $\delta_{\text{NS}}^{(0)}\|_{\text{mag+LS}}$	$-[0.406, 0.443]$ [165]
H&T 2020 [4]	$-0.400(35)(36)$
H&T 2014 [23]	$-0.345(35)$

As detailed in Ref. [31] for the $^{10}\text{C} \to {}^{10}\text{B}$ transition, the central value for δ_{NS} in the CA formalism is obtained by averaging over two realistic, different-order chiral interactions at fixed harmonic oscillator frequency, while the uncertainty combines the many-body truncation, multipole truncation, one-nucleon form-factor dependence, subtraction of the

elastic single-nucleon γW box, chiral truncation, residual oscillator-frequency dependence, and the so-called nuclear-shadowing uncertainty [172–175]. The prediction from the more rigorous calculation agrees with the most recently adopted value for the $^{10}\mathrm{C} \to {}^{10}\mathrm{B}$ decay in the Hardy and Towner 2020 critical survey of superallowed decays [4]; the uncertainty is further reduced by a factor of 1.6× back to its estimated 2014 value, despite the inclusion of the largely unconstrained nuclear shadowing effects in the uncertainty budget. Unfortunately, Bayesian analyses are presently prohibitive. Such nuclear shadowing effects, along with the lack of inclusion of two-body currents in the current-algebra calculation, represent the largest contributors to the nuclear many-body uncertainty in this formalism. While the errors are quantified, their estimation is ad hoc and overly conservative. Thus, follow-up studies on their sizes and impact—particularly for the latter—are critical to push beyond the present-order-of-magnitude uncertainty regime established by the Hardy and Towner studies. There exist proposals to target the missing two-body currents, with development presently underway.

The complementary treatment recently developed in Refs. [164,165,170] sees the nucleus-dependent radiative corrections relevant for $\mathcal{O}(10^{-4})$ precision derived from a tower of EFTs running from the electroweak scale to hadronic and nuclear scales. In contrast to the current algebra formalism, which targets a "direct" SM calculation—notably by combining pieces of the hadronic γW box modeling with the corresponding pieces in a point-like-nucleon model of nuclei, along with explicit responses of the intermediate nuclear spectrum—the EFT approach separates hard, soft, potential, and ultrasoft photon modes according to the hierarchy of scales $|\mathbf{q}_{\mathrm{ext}}| \sim m_e \ll m_\pi \ll \Lambda_\chi \ll M_W$. Many formal developments of this approach began with the treatment of electromagnetic bound states in potential non-relativistic quantum electrodynamics [176–179]. This allows for a transparent factorization of the decay rate at the desired precision. The short-range contribution is governed by two presently unknown low-energy constants, denoted as g_{V1}^{NN} and g_{V2}^{NN}, so the framework is systematic but not parameter-free. These constants may be obtained either from matching to QCD or, possibly, from a fit to several precisely measured superallowed transitions. With this approach in a given many-body method, one merely needs to evaluate two-body amplitudes between the relevant initial and final states to predict the complete radiative correction $\bar{\delta}_{\mathrm{NS}}^{E}$. We include results for the $^{10}\mathrm{C} \to {}^{10}\mathrm{B}$ transition as taken from the second of two independent studies in this formalism using Quantum Monte Carlo (QMC) approaches; the study on the $^{14}\mathrm{O} \to {}^{14}\mathrm{N}$ decay is not readily comparable to the historical values. The quoted value contains only the long-range part of the correction since this approximately maps onto the current algebra formalism. The overall uncertainty in $\bar{\delta}_{\mathrm{NS}}^{E}$ is dominated by the unknown short-range couplings that a rigorous fit could reduce to $\delta V_{ud} \sim 3 \times 10^{-4}$, competitive with that of the current algebra calculation.

The impact on V_{ud} is, therefore, twofold. First, the current algebra calculation reduces the theory uncertainty assigned to the lightest superallowed Fermi transition, where the radiative correction is the central limitation on the corrected $\mathcal{F}t$ value. Second, the shift of all modern calculations relative to historical evaluations changes the inferred degree of consistency among superallowed emitters and hence the weight carried by $^{10}\mathrm{C} \to {}^{10}\mathrm{B}$ and $^{14}\mathrm{O} \to {}^{14}\mathrm{N}$ in tests of CKM unitarity. This is doubly important because the light decays $^{10}\mathrm{C} \to {}^{10}\mathrm{B}$ and $^{14}\mathrm{O} \to {}^{14}\mathrm{N}$ are by far the most sensitive to possible scalar-current extensions of the SM [4]. The promise of further improvements to theory extractions of radiative corrections also clarifies the target for experiment. For $^{10}\mathrm{C}$, the dominant experimental limitation remains the branching ratio. Coupled with the reduction in radiative correction uncertainties, a new high-precision branching-ratio measurement would, therefore, feed into (i) improving the contribution of the $^{10}\mathrm{C} \to {}^{10}\mathrm{B}$ to a more competitive determination of V_{ud}, and (ii) enforcing increasingly strict constraints on scalar extensions of the SM.

Proposed recoil-detection approaches, including superconducting tunnel junction measurements inspired by successful ^{7}Be electron-capture studies [180–182], and trapped-ion recoil programs sensitive to exotic β-decay currents [183,184], are already occurring in this direction. In the next decade, improved theory and targeted measurements become tightly coupled ingredients in extracting V_{ud} with higher and higher precision in motion toward the ultimate goal of resolving the Cabibbo anomaly.

6. Conclusions and Future Directions

Today, several precision tests of the Standard Model at the low-energy frontier are limited by nuclear-structure theory and its associated uncertainties. In this review, we have discussed the leading nuclear-structure corrections entering two such programs—the two-photon-exchange contribution to the muonic Lamb shift and the γW box radiative correction to superallowed decays—and shown that they are two faces of a single theoretical coin: the generalized hadronic tensor of Section 2. The modern *ab initio* approach, rooted in χEFT Hamiltonians and consistent electroweak currents along with Bayesian uncertainty quantification, has turned the evaluation of nuclear electroweak correlators from model-dependent estimates into systematically improvable calculations.

The dividends of such progress are visible in the milestones reviewed herein. In muonic atoms (Section 4), the N^{3}LO computation of the two-photon-exchange corrections in muonic-helium ions, equipped with Bayesian truncation errors, enabled precise determinations of the helion and α-particle charge radii [15,16,18,22]. For the helium isotope-shift puzzle, these rigorously quantified uncertainties clearly excluded nuclear structure corrections as the origin of the 4σ tension and directed the scrutiny toward atomic theory, where the missing contributions were ultimately found [19,20]. This puzzle was thus resolved without the need to invoke new physics. In superallowed β decays (Section 5), a first-of-its-kind *ab initio* computation of the nuclear γW box for the lightest transition, $^{10}\mathrm{C} \to {}^{10}\mathrm{B}$ [31], re-sharpened the evaluation of the nuclear-structure-dependent correction that dominates the V_{ud} uncertainty budget [4,5] and established a systematically improvable approach towards confronting the 2–3σ tension in top-row CKM unitarity test [5,7].

The road ahead still presents several challenges. On the side of methodology, fully uncertainty-quantified predictions require propagating the statistical uncertainties of the low-energy constants of χEFT into electroweak observables. At the moment, this is only feasible with reduced-order emulators such as eigenvector continuation (Section 3.3). Greater precision further requires the inclusion of electroweak currents at higher chiral orders via consistent expansion of both electroweak currents and nuclear Hamiltonians in χEFT, as well as computational advances to render larger model spaces accessible. On the physics side, experiment sets the agenda. The QUARTET and muX programs [33,34,124,125] are working to extend muonic-atom spectroscopy beyond the light-mass region, where nuclear polarization remains the limiting theoretical input and bridging exact *ab initio* methods with the mean-field-based approaches of heavier systems [126,129] is a significant challenge. Another important observable pursued by the CREMA collaboration is the hyperfine splitting [185], which likewise requires nuclear-structure input, but of a spin-dependent nature that is considerably more challenging to compute [186–188]. For superallowed decays, the completion of the $^{14}\mathrm{O} \to {}^{14}\mathrm{N}$ analysis and the extension to heavier emitters such as ^{18}Ne, ^{22}Mg, and ^{26m}Al, together with *ab initio* evaluations of the isospin-symmetry-breaking correction δ_C, will determine whether the unitarity deficit survives such improvements from theory. Indeed, the two programs reviewed here already intersect in this arena: the charge radii entering the ^{26m}Al analysis are themselves obtained from muonic X-ray spec-

troscopy, and an updated nuclear polarization correction has recently been shown to reduce the CKM unitarity deficit by one standard deviation [32].

Notably, the same machinery discussed in this review readily generalizes to (i) the γZ box, which enters weak-charge measurements, (ii) to muon capture, a process with strong connections to neutrinoless double-β decay, and (iii) to neutrino-nucleus scattering. With percent-level, statistically meaningful control over electroweak processes in nuclei within reach, low-energy precision experiments stand as competitive and complementary probes to direct searches at colliders, sensitive to new physics at scales of 10 TeV and beyond.

Author Contributions: The authors have contributed equally to the preparation of this review. All authors have read and agreed to the published version of the manuscript.

Funding: This work was supported by the Swedish Research Council via a Research Project Grant, No. 2021-04507, and by a Tage Erlander Visiting Professorship, Grant No. 2022-00215 (SSLM). This work was supported in part by the Deutsche Forschungsgemeinschaft (DFG) through the Cluster of Excellence "Precision Physics, Fundamental Interactions, and Structure of Matter" (Project ID 390831469) (MG).

Data Availability Statement: No new data were created or analyzed in this study. Data sharing is not applicable to this article.

Acknowledgments: We thank Chien-Yeah Seng, Wouter Dekens, Petr Navvratil, Ben Ohayon, Franziska Hagelstein and Vadim Lensky for helpful comments on the manuscript.

Conflicts of Interest: The authors declare no conflicts of interest.

References

1. Cirgiliano, V.; Garcia, A.; Gazit, D.; Naviliat-Cuncic, O.; Savard, G.; Young, A. Precision Beta Decay as a Probe of New Physics. *arXiv* **2019**, arXiv:1907.02164.
2. Brodeur, M.; Buzinsky, N.; Caprio, M.A.; Cirigliano, V.; Clark, J.A.; Fasano, P.J.; Formaggio, J.A.; Gallant, A.T.; Garcia, A.; Gandolfi, S.; et al. Nuclear β decay as a probe for physics beyond the Standard Model. *arXiv* **2023**, arXiv:2301.03975.
3. Safronova, M.S.; Budker, D.; DeMille, D.; Kimball, D.F.J.; Derevianko, A.; Clark, C.W. Search for new physics with atoms and molecules. *Rev. Mod. Phys.* **2018**, *90*, 025008. [CrossRef]
4. Hardy, J.C.; Towner, I.S. Superallowed $0^+ \to 0^+$ nuclear β decays: 2020 critical survey, with implications for V_{ud} and CKM unitarity. *Phys. Rev. C* **2020**, *102*, 045501. [CrossRef]
5. Gorchtein, M.; Seng, C.Y. Superallowed Nuclear Beta Decays and Precision Tests of the Standard Model. *Annu. Rev. Nucl. Part. Sci.* **2024**, *74*, 23–47. [CrossRef]
6. Seng, C.Y.; Gorchtein, M.; Patel, H.H.; Ramsey-Musolf, M.J. Reduced Hadronic Uncertainty in the Determination of V_{ud}. *Phys. Rev. Lett.* **2018**, *121*, 241804. [CrossRef]
7. Navas, S.; Amsler, C.; Gutsche, T.; Hanhart, C.; Lourenço, C.; Masoni, A.; Mikhasenko, M.; Mitchell, R.; Patrignani, C.; Schwanda, C.; et al. Review of Particle Physics. *Phys. Rev. D* **2024**, *110*, 030001. [CrossRef]
8. Glick-Magid, A.; Forssén, C.; Gazda, D.; Gazit, D.; Gysbers, P.; Navrátil, P. Nuclear *ab initio* calculations of ^{6}He β-decay for beyond the Standard Model studies. *Phys. Lett. B* **2022**, *832*, 137259. [CrossRef]
9. King, G.B.; Baroni, A.; Cirigliano, V.; Gandolfi, S.; Hayen, L.; Mereghetti, E.; Pastore, S.; Piarulli, M. *Ab initio* calculation of the β-decay spectrum of ^{6}He. *Phys. Rev. C* **2023**, *107*, 015503. [CrossRef]
10. Pachucki, K.; Lensky, V.; Hagelstein, F.; Li Muli, S.S.; Bacca, S.; Pohl, R. Comprehensive theory of the Lamb shift in light muonic atoms. *Rev. Mod. Phys.* **2024**, *96*, 015001. [CrossRef]
11. Antognini, A.; Bacca, S.; Fleischmann, A.; Gastaldo, L.; Hagelstein, F.; Indelicato, P.; Knecht, A.; Lensky, V.; Ohayon, B.; Pascalutsa, V.; et al. Muonic-Atom Spectroscopy and Impact on Nuclear Structure and Precision QED Theory. *arXiv* **2022**, arXiv:2210.16929.
12. Pohl, R.; Antognini, A.; Nez, F.; Amaro, F.D.; Biraben, F.; Cardoso, J.M.; Covita, D.S.; Dax, A.; Dhawan, S.; Fernandes, L.M.; et al. The size of the proton. *Nature* **2010**, *466*, 213–216. [CrossRef]
13. Antognini, A.; Nez, F.; Schuhmann, K.; Amaro, F.D.; Biraben, F.; Cardoso, J.M.; Covita, D.S.; Dax, A.; Dhawan, S.; Diepold, M.; et al. Proton Structure from the Measurement of 2S-2P Transition Frequencies of Muonic Hydrogen. *Science* **2013**, *339*, 417–420. [CrossRef]
14. Tiesinga, E.; Mohr, P.J.; Newell, D.B.; Taylor, B.N. CODATA recommended values of the fundamental physical constants: 2018. *Rev. Mod. Phys.* **2021**, *93*, 025010. [CrossRef]

15. Krauth, J.J.; Schuhmann, K.; Ahmed, M.A.; Amaro, F.D.; Amaro, P.; Biraben, F.; Chen, T.L.; Covita, D.S.; Dax, A.J.; Diepold, M.; et al. Measuring the α-particle charge radius with muonic helium-4 ions. *Nature* **2021**, *589*, 527–531. [CrossRef]
16. Schuhmann, K.; Fernandes, L.M.P.; Nez, F.; Ahmed, M.A.; Amaro, F.D.; Amaro, P.; Biraben, F.; Chen, T.L.; Covita, D.S.; Dax, A.J.; et al. The helion charge radius from laser spectroscopy of muonic helium-3 ions. *Science* **2025**, *388*, 854–858. [CrossRef]
17. van der Werf, Y.; Steinebach, K.; Jannin, R.; Bethlem, H.L.; Eikema, K.S.E. The alpha and helion particle charge radius difference from spectroscopy of quantum-degenerate helium. *arXiv* **2023**, arXiv:2306.02333.
18. Li Muli, S.S.; Richardson, T.R.; Bacca, S. Revisiting the Helium Isotope-Shift Puzzle with Improved Uncertainties from Nuclear Structure Corrections. *Phys. Rev. Lett.* **2025**, *134*, 032502. [CrossRef]
19. Qi, X.Q.; Zhang, P.P.; Yan, Z.C.; Tang, L.Y.; Chen, A.X.; Shi, T.Y.; Zhong, Z.X. Toward resolving the discrepancy in helium-3 and helium-4 nuclear charge radii. *Phys. Rev. Res.* **2025**, *7*, L022020. [CrossRef]
20. Pachucki, K.; Patkóš, V.; Yerokhin, V.A. Second-order hyperfine correction to H, D, and ^{3}He energy levels. *Phys. Rev. A* **2024**, *110*, 062806. [CrossRef]
21. Rathi, S.; Jentschura, U.D.; Indelicato, P.; Ohayon, B. Binding energy of muonic beryllium: Perturbative versus all-order calculations. *J. Phys. B At. Mol. Opt. Phys.* **2026**, *59*, 125002. [CrossRef]
22. Ji, C.; Bacca, S.; Barnea, N.; Hernandez, O.J.; Dinur, N.N. *Ab initio* calculation of nuclear-structure corrections in muonic atoms. *J. Phys. G Nucl. Part. Phys.* **2018**, *45*, 093002. [CrossRef]
23. Hardy, J.C.; Towner, I.S. Superallowed $0^+ \to 0^+$ nuclear β decays: 2014 critical survey, with precise results for V_{ud} and CKM unitarity. *Phys. Rev. C* **2015**, *91*, 025501. [CrossRef]
24. Gorchtein, M. γW Box Inside Out: Nuclear Polarizabilities Distort the Beta Decay Spectrum. *Phys. Rev. Lett.* **2019**, *123*, 042503. [CrossRef]
25. Epelbaum, E.; Hammer, H.W.; Meißner, U.G. Modern theory of nuclear forces. *Rev. Mod. Phys.* **2009**, *81*, 1773–1825. [CrossRef]
26. Machleidt, R.; Entem, D. Chiral effective field theory and nuclear forces. *Phys. Rep.* **2011**, *503*, 1–75. [CrossRef]
27. Hammer, H.W.; König, S.; van Kolck, U. Nuclear effective field theory: Status and perspectives. *Rev. Mod. Phys.* **2020**, *92*, 025004. [CrossRef]
28. Hergert, H. A Guided Tour of *ab initio* Nuclear Many-Body Theory. *Front. Phys.* **2020**, *8*, 379. [CrossRef]
29. Furnstahl, R.J.; Klco, N.; Phillips, D.R.; Wesolowski, S. Quantifying truncation errors in effective field theory. *Phys. Rev. C* **2015**, *92*, 024005. [CrossRef]
30. Melendez, J.A.; Furnstahl, R.J.; Phillips, D.R.; Pratola, M.T.; Wesolowski, S. Quantifying correlated truncation errors in effective field theory. *Phys. Rev. C* **2019**, *100*, 044001. [CrossRef]
31. Gennari, M.; Drissi, M.; Gorchtein, M.; Navrátil, P.; Seng, C.Y. *Ab Initio* Strategy for Taming the Nuclear-Structure Dependence of V_{ud} Extractions: The ^{10}C $\to$ ^{10}B Superallowed Transition. *Phys. Rev. Lett.* **2025**, *134*, 012501. [CrossRef]
32. Gorchtein, M.; Katyal, V.; Ohayon, B.; Sahoo, B.K.; Seng, C.Y. Cabibbo-Kobayashi-Maskawa unitarity deficit reduction via finite nuclear size. *Phys. Rev. Res.* **2025**, *7*, L042002. [CrossRef]
33. Ohayon, B.; Abeln, A.; Bara, S.; Cocolios, T.E.; Eizenberg, O.; Fleischmann, A.; Gastaldo, L.; Godinho, C.; Heines, M.; Hengstler, D.; et al. Towards Precision Muonic X-Ray Measurements of Charge Radii of Light Nuclei. *Physics* **2024**, *6*, 206–215. [CrossRef]
34. Unger, D.; Abeln, A.; Cocolios, T.E.; Eizenberg, O.; Enss, C.; Fleischmann, A.; Gastaldo, L.; Godinho, C.; Heines, M.; Hengstler, D.; et al. MMC Array to Study X-Ray Transitions in Muonic Atoms. *J. Low Temp. Phys.* **2024**, *216*, 344–351. [CrossRef]
35. Beyer, K.A.; Cocolios, T.E.; Costache, C.; Demol, P.; Deseyn, M.; Doinaki, A.; Eizenberg, O.; Gorchtein, M.; Heines, M.; Herzáň, A.; et al. Charge radii of Cl isotopes from x-ray spectroscopy of muonic atoms. *arXiv* **2026**, arXiv:2605.08413.
36. Eizenberg, O.; Rathi, S.; Abeln, A.; Bacca, S.; Baptista, G.; Barnea, N.; Burger, N.; Cocolios, T.E.; Deseyn, M.; Egert, T.; et al. Nuclear Charge Radius of ^{9}Be from Muonic Atom Spectroscopy Using a Microcalorimeter. *arXiv* **2026**, arXiv:2607.13690.
37. Carlson, C.E.; Vanderhaeghen, M. Higher-order proton structure corrections to the Lamb shift in muonic hydrogen. *Phys. Rev. A* **2011**, *84*, 020102. [CrossRef]
38. Antognini, A.; Hagelstein, F.; Pascalutsa, V. The Proton Structure in and out of Muonic Hydrogen. *Annu. Rev. Nucl. Part. Sci.* **2022**, *72*, 389–418. [CrossRef]
39. Krebs, H. Nuclear currents in chiral effective field theory. *Eur. Phys. J. A* **2020**, *56*, 234. [CrossRef]
40. Walecka, J.D. *Theoretical Nuclear and Subnuclear Physics*, 2nd ed.; World Scientific: Singapore; Imperial College Press: London, UK, 2004. [CrossRef]
41. Donnelly, T.; Haxton, W. Multipole operators in semileptonic weak and electromagnetic interactions with nuclei: Harmonic oscillator single-particle matrix elements. *At. Data Nucl. Data Tables* **1979**, *23*, 103–176. [CrossRef]
42. Haxton, W.; Lunardini, C. SevenOperators, a Mathematica script for harmonic oscillator nuclear matrix elements arising in semileptonic electroweak interactions. *Comput. Phys. Commun.* **2008**, *179*, 345–358. [CrossRef]
43. Wiringa, R.B.; Stoks, V.G.J.; Schiavilla, R. Accurate nucleon-nucleon potential with charge-independence breaking. *Phys. Rev. C* **1995**, *51*, 38–51. [CrossRef]
44. Machleidt, R. High-precision, charge-dependent Bonn nucleon-nucleon potential. *Phys. Rev. C* **2001**, *63*, 024001. [CrossRef]

45. Pudliner, B.S.; Pandharipande, V.R.; Carlson, J.; Wiringa, R.B. Quantum Monte Carlo Calculations of $A \leq 6$ Nuclei. *Phys. Rev. Lett.* **1995**, *74*, 4396–4399. [CrossRef]
46. Pieper, S.C.; Pandharipande, V.R.; Wiringa, R.B.; Carlson, J. Realistic models of pion-exchange three-nucleon interactions. *Phys. Rev. C* **2001**, *64*, 014001. [CrossRef]
47. Weinberg, S. Nuclear forces from chiral Lagrangians. *Phys. Lett. B* **1990**, *251*, 288–292. [CrossRef]
48. Weinberg, S. Effective chiral Lagrangians for nucleon-pion interactions and nuclear forces. *Nucl. Phys. B* **1991**, *363*, 3–18. [CrossRef]
49. Weinberg, S. Three-body interactions among nucleons and pions. *Phys. Lett. B* **1992**, *295*, 114–121. [CrossRef]
50. Epelbaum, E.; Krebs, H.; Meißner, U.G. Precision Nucleon-Nucleon Potential at Fifth Order in the Chiral Expansion. *Phys. Rev. Lett.* **2015**, *115*, 122301. [CrossRef]
51. Epelbaum, E.; Krebs, H.; Reinert, P. High-Precision Nuclear Forces From Chiral EFT: State-of-the-Art, Challenges, and Outlook. *Front. Phys.* **2020**, *8*, 98. [CrossRef]
52. Piarulli, M.; Girlanda, L.; Schiavilla, R.; Navarro Pérez, R.; Amaro, J.E.; Ruiz Arriola, E. Minimally nonlocal nucleon-nucleon potentials with chiral two-pion exchange including Δ resonances. *Phys. Rev. C* **2015**, *91*, 024003. [CrossRef]
53. Thim, O.; Ekström, A.; Forssén, C. Perturbative calculations of light nuclei up to N^3LO in chiral effective field theory. *arXiv* **2026**, arXiv:2604.14985.
54. Thim, O. Chiral Effective Field Theory with Partly Perturbative Pions Applied to the Few-Nucleon Sector. Ph.D. Thesis, Chalmers University of Technology, Gothenburg, Sweden, 2026. [CrossRef]
55. Gezerlis, A.; Tews, I.; Epelbaum, E.; Freunek, M.; Gandolfi, S.; Hebeler, K.; Nogga, A.; Schwenk, A. Local chiral effective field theory interactions and quantum Monte Carlo applications. *Phys. Rev. C* **2014**, *90*, 054323. [CrossRef]
56. Lynn, J.E.; Tews, I.; Carlson, J.; Gandolfi, S.; Gezerlis, A.; Schmidt, K.E.; Schwenk, A. Chiral Three-Nucleon Interactions in Light Nuclei, Neutron-α Scattering and Neutron Matter. *Phys. Rev. Lett.* **2016**, *116*, 062501. [CrossRef]
57. Piarulli, M.; Tews, I. Local Nucleon-Nucleon and Three-Nucleon Interactions Within Chiral Effective Field Theory, and Neutron Matter. *Front. Phys.* **2020**, *7*, 245. [CrossRef]
58. Somasundaram, R.; Lynn, J.E.; Huth, L.; Schwenk, A.; Tews, I. Maximally local two-nucleon interactions at N^3LO in Δ-less chiral effective field theory. *Phys. Rev. C* **2024**, *109*, 034005. [CrossRef]
59. Li Muli, S.S.; Bacca, S.; Barnea, N. Implementation of Local Chiral Interactions in the Hyperspherical Harmonics Formalism. *Front. Phys.* **2021**, *9*, 671869. [CrossRef]
60. Pastore, S.; Baroni, A.; Carlson, J.; Gandolfi, S.; Pieper, S.C.; Schiavilla, R.; Wiringa, R.B. Quantum Monte Carlo calculations of weak transitions in $A = 6$–10 nuclei. *Phys. Rev. C* **2018**, *97*, 022501. [CrossRef]
61. King, G.B.; Andreoli, L.; Pastore, S.; Piarulli, M.; Schiavilla, R.; Wiringa, R.B.; Carlson, J.; Gandolfi, S. Chiral effective field theory calculations of weak transitions in light nuclei. *Phys. Rev. C* **2020**, *102*, 025501. [CrossRef]
62. Li Muli, S.S.; Djärv, T.R.; Forssén, C.; Phillips, D.R. Role of Spin-Isospin Symmetries in Nuclear β-Decays. *Phys. Rev. Lett.* **2026**, *136*, 242501. [CrossRef]
63. Carlson, J.; Gandolfi, S.; Pederiva, F.; Pieper, S.C.; Schiavilla, R.; Schmidt, K.E.; Wiringa, R.B. Quantum Monte Carlo methods for nuclear physics. *Rev. Mod. Phys.* **2015**, *87*, 1067–1118. [CrossRef]
64. Lynn, J.E.; Tews, I.; Carlson, J.; Gandolfi, S.; Gezerlis, A.; Schmidt, K.E.; Schwenk, A. Quantum Monte Carlo calculations of light nuclei with local chiral two- and three-nucleon interactions. *Phys. Rev. C* **2017**, *96*, 054007. [CrossRef]
65. Lonardoni, D.; Gandolfi, S.; Lynn, J.E.; Petrie, C.; Carlson, J.; Schmidt, K.E.; Schwenk, A. Auxiliary field diffusion Monte Carlo calculations of light and medium-mass nuclei with local chiral interactions. *Phys. Rev. C* **2018**, *97*, 044318. [CrossRef]
66. Viviani, M.; Marcucci, L.E.; Rosati, S.; Kievsky, A.; Girlanda, L. Variational Calculation on A = 3 and 4 Nuclei with Non-Local Potentials. *Few-Body Syst.* **2006**, *39*, 159–176. [CrossRef]
67. Marcucci, L.E.; Dohet-Eraly, J.; Girlanda, L.; Gnech, A.; Kievsky, A.; Viviani, M. The hyperspherical harmonics method: A tool for testing and improving nuclear interaction models. *Front. Phys.* **2020**, *8*, 69. [CrossRef]
68. Barnea, N.; Leidemann, W.; Orlandini, G. State dependent effective interaction for the hyperspherical formalism. *Phys. Rev. C* **2000**, *61*, 054001. [CrossRef]
69. Barrett, B.R.; Navrátil, P.; Vary, J.P. *Ab initio* no core shell model. *Prog. Part. Nucl. Phys.* **2013**, *69*, 131–181. [CrossRef]
70. Hagen, G.; Papenbrock, T.; Hjorth-Jensen, M.; Dean, D.J. Coupled-cluster computations of atomic nuclei. *Rep. Prog. Phys.* **2014**, *77*, 096302. [CrossRef]
71. Hergert, H.; Bogner, S.; Morris, T.; Schwenk, A.; Tsukiyama, K. The In-Medium Similarity Renormalization Group: A novel *ab initio* method for nuclei. *Phys. Rep.* **2016**, *621*, 165–222. [CrossRef]
72. Lanczos, C. An iteration method for the solution of the eigenvalue problem of linear differential and integral operators. *J. Res. Natl. Bur. Stand.* **1950**, *45*, 255–282. [CrossRef]
73. Komzsik, L. *The Lanczos Method: Evolution and Application*; SIAM: Philadelphia, PA, USA, 2003.

74. Paige, C. Accuracy and effectiveness of the Lanczos algorithm for the symmetric eigenproblem. *Linear Algebra Its Appl.* **1980**, *34*, 235–258. [CrossRef]
75. Parlett, B.N. Do we fully understand the symmetric Lanczos algorithm yet? In *Proceedings of the Cornelius Lanczos International Centenary Conference, Raleigh, NC, USA, 12–17 December 1993*; SIAM: Philadelphia, PA, USA, 1994; pp. 93–107.
76. Haydock, R. The inverse of a linear operator. *J. Phys. A Math. Nucl. Gen.* **1974**, *7*, 2120–2124. [CrossRef]
77. Haydock, R. The Recursive Solution of the Schrodinger Equation. In *Solid State Physics*; Ehrenreich, H., Seitz, F., Turnbull, D., Eds.; Academic Press: Cambridge, MA, USA, 1980; Volume 35, pp. 215–294. [CrossRef]
78. Heine, V. Electronic Structure from the Point of View of the Local Atomic Environment. In *Solid State Physics*; Ehrenreich, H., Seitz, F., Turnbull, D., Eds.; Academic Press: Cambridge, MA, USA, 1980; Volume 35, pp. 1–127. [CrossRef]
79. Kelly, M. Applications of the Recursion Method to the Electronic Structure from an Atomic Point of View. In *Solid State Physics*; Ehrenreich, H., Seitz, F., Turnbull, D., Eds.; Academic Press: Cambridge, MA, USA, 1980; Volume 35, pp. 295–383. [CrossRef]
80. Haydock, R.; Heine, V.; Kelly, M.J. Electronic structure based on the local atomic environment for tight-binding bands. *J. Phys. C Solid State Phys.* **1972**, *5*, 2845. [CrossRef]
81. Pettifor, D.G.; Weaire, D.L. *The Recursion Method and Its Applications: Proceedings of the Conference, Imperial College, London, England September 13–14. 1984*; Springer Science & Business Media: Berlin/Heidelberg, Germany, 2012; Volume 58.
82. Marchisio, M.; Barnea, N.; Leidemann, W.; Orlandini, G. Efficient method for Lorentz integral transforms of reaction cross sections. *Few-Body Syst.* **2003**, *33*, 259–276. [CrossRef]
83. Haxton, W.C.; Nollett, K.M.; Zurek, K.M. Piecewise moments method: Generalized Lanczos technique for nuclear response surfaces. *Phys. Rev. C* **2005**, *72*, 065501. [CrossRef]
84. Nevo Dinur, N.; Barnea, N.; Ji, C.; Bacca, S. Efficient method for evaluating energy-dependent sum rules. *Phys. Rev. C* **2014**, *89*, 064317. [CrossRef]
85. Hao, Y.; Navrátil, P.; Norrgard, E.B.; Iliaš, M.; Eliav, E.; Timmermans, R.G.E.; Flambaum, V.V.; Borschevsky, A. Nuclear spin-dependent parity-violating effects in light polyatomic molecules. *Phys. Rev. A* **2020**, *102*, 052828. [CrossRef]
86. Froese, P.; Navrátil, P. *Ab initio* calculations of electric dipole moments of light nuclei. *Phys. Rev. C* **2021**, *104*, 025502. [CrossRef]
87. Dagotto, E. Correlated electrons in high-temperature superconductors. *Rev. Mod. Phys.* **1994**, *66*, 763–840. [CrossRef]
88. Bessis, D.; Villani, M. Perturbative-variational approximations to the spectral properties of semibounded Hilbert space operators, based on the moment problem with finite or diverging moments. Application to quantum mechanical systems. *J. Math. Phys.* **1975**, *16*, 462–474. [CrossRef]
89. Li Muli, S.S. Nuclear Structure Corrections in Muonic Atoms. Ph.D. Thesis, Johannes Gutenberg-Universität Mainz, Mainz, Germany, 2023. [CrossRef]
90. Ekström, A. Analyzing the Nuclear Interaction: Challenges and New Ideas. *Front. Phys.* **2020**, *8*, 29. [CrossRef]
91. Melendez, J.A.; Wesolowski, S.; Furnstahl, R.J. Bayesian truncation errors in chiral effective field theory: Nucleon-nucleon observables. *Phys. Rev. C* **2017**, *96*, 024003. [CrossRef]
92. Schindler, M.; Phillips, D. Bayesian methods for parameter estimation in effective field theories. *Ann. Phys.* **2009**, *324*, 682–708. [CrossRef]
93. Wesolowski, S.; Furnstahl, R.J.; Melendez, J.A.; Phillips, D.R. Exploring Bayesian parameter estimation for chiral effective field theory using nucleon–nucleon phase shifts. *J. Phys. G Nucl. Part. Phys.* **2019**, *46*, 045102. [CrossRef]
94. Svensson, I.; Ekström, A.; Forssén, C. Bayesian estimation of the low-energy constants up to fourth order in the nucleon-nucleon sector of chiral effective field theory. *Phys. Rev. C* **2023**, *107*, 014001. [CrossRef]
95. Wesolowski, S.; Svensson, I.; Ekström, A.; Forssén, C.; Furnstahl, R.J.; Melendez, J.A.; Phillips, D.R. Rigorous constraints on three-nucleon forces in chiral effective field theory from fast and accurate calculations of few-body observables. *Phys. Rev. C* **2021**, *104*, 064001. [CrossRef]
96. Frame, D.; He, R.; Ipsen, I.; Lee, D.; Lee, D.; Rrapaj, E. Eigenvector Continuation with Subspace Learning. *Phys. Rev. Lett.* **2018**, *121*, 032501. [CrossRef]
97. König, S.; Ekström, A.; Hebeler, K.; Lee, D.; Schwenk, A. Eigenvector continuation as an efficient and accurate emulator for uncertainty quantification. *Phys. Lett. B* **2020**, *810*, 135814. [CrossRef]
98. Djärv, T.; Ekström, A.; Forssén, C.; Johansson, H.T. Bayesian predictions for $A = 6$ nuclei using eigenvector continuation emulators. *Phys. Rev. C* **2022**, *105*, 014005. [CrossRef]
99. Acharya, B.; Bacca, S.; Bonaiti, F.; Li Muli, S.S.; Sobczyk, J.E. Uncertainty quantification in electromagnetic observables on nuclei. *Front. Phys.* **2023**, *10*, 1066035. [CrossRef]
100. Pohl, R.; Nez, F.; Fernandes, L.M.; Amaro, F.D.; Biraben, F.; Cardoso, J.M.; Covita, D.S.; Dax, A.; Dhawan, S.; Diepold, M.; et al. Laser spectroscopy of muonic deuterium. *Science* **2016**, *353*, 669–673. [CrossRef]
101. Nevado, D.; Pineda, A. Forward virtual Compton scattering and the Lamb shift in chiral perturbation theory. *Phys. Rev. C* **2008**, *77*, 035202. [CrossRef]

102. Peset, C.; Pineda, A. The two-photon exchange contribution to muonic hydrogen from chiral perturbation theory. *Nucl. Phys. B* **2014**, *887*, 69–111. [CrossRef]
103. Birse, M.C.; McGovern, J.A. Proton polarisability contribution to the Lamb shift in muonic hydrogen at fourth order in chiral perturbation theory. *Eur. Phys. J. A* **2012**, *48*, 120. [CrossRef]
104. Alarcón, J.M.; Lensky, V.; Pascalutsa, V. Chiral perturbation theory of muonic-hydrogen Lamb shift: Polarizability contribution. *Eur. Phys. J. C* **2014**, *74*, 2852. [CrossRef]
105. Friar, J.L. Nuclear polarization corrections to μ-d atoms in zero-range approximation. *Phys. Rev. C* **2013**, *88*, 034003. [CrossRef]
106. Pachucki, K. Nuclear Structure Corrections in Muonic Deuterium. *Phys. Rev. Lett.* **2011**, *106*, 193007. [CrossRef]
107. Pachucki, K.; Wienczek, A. Nuclear structure effects in light muonic atoms. *Phys. Rev. A* **2015**, *91*, 040503. [CrossRef]
108. Hernandez, O.; Ji, C.; Bacca, S.; Nevo Dinur, N.; Barnea, N. Improved estimates of the nuclear structure corrections in μD. *Phys. Lett. B* **2014**, *736*, 344–349. [CrossRef]
109. Hernandez, O.J.; Ekström, A.; Nevo Dinur, N.; Ji, C.; Bacca, S.; Barnea, N. The deuteron-radius puzzle is alive: A new analysis of nuclear structure uncertainties. *Phys. Lett. B* **2018**, *778*, 377–383. [CrossRef]
110. Hernandez, O.J.; Ji, C.; Bacca, S.; Barnea, N. Probing uncertainties of nuclear structure corrections in light muonic atoms. *Phys. Rev. C* **2019**, *100*, 064315. [CrossRef]
111. Kalinowski, M. Deuteron charge radius from the Lamb-shift measurement in muonic deuterium. *Phys. Rev. A* **2019**, *99*, 030501. [CrossRef]
112. Acharya, B.; Lensky, V.; Bacca, S.; Gorchtein, M.; Vanderhaeghen, M. Dispersive evaluation of the Lamb shift in muonic deuterium from chiral effective field theory. *Phys. Rev. C* **2021**, *103*, 024001. [CrossRef]
113. Lensky, V.; Hagelstein, F.; Pascalutsa, V. A reassessment of nuclear effects in muonic deuterium using pionless effective field theory at N3LO. *Phys. Lett. B* **2022**, *835*, 137500. [CrossRef]
114. Lensky, V.; Hagelstein, F.; Pascalutsa, V. Two-photon exchange in (muonic) deuterium at N3LO in pionless effective field theory. *Eur. Phys. J. A* **2022**, *58*, 224. [CrossRef]
115. Carlson, C.E.; Gorchtein, M.; Vanderhaeghen, M. Nuclear-structure contribution to the Lamb shift in muonic deuterium. *Phys. Rev. A* **2014**, *89*, 022504. [CrossRef]
116. Nevo Dinur, N.; Ji, C.; Bacca, S.; Barnea, N. Nuclear structure corrections to the Lamb shift in μ^3He$^+$ and μ^3H. *Phys. Lett. B* **2016**, *755*, 380–386. [CrossRef]
117. Ji, C.; Nevo Dinur, N.; Bacca, S.; Barnea, N. Nuclear Polarization Corrections to the μ^4He$^+$ Lamb Shift. *Phys. Rev. Lett.* **2013**, *111*, 143402. [CrossRef]
118. Li Muli, S.S.; Acharya, B.; Hernandez, O.J.; Bacca, S. Bayesian analysis of nuclear polarizability corrections to the Lamb shift of muonic H-atoms and He-ions. *J. Phys. G* **2022**, *49*, 105101. [CrossRef]
119. Friar, J.L. Nuclear polarization corrections in $\mu - {}^4$He atoms. *Phys. Rev. C* **1977**, *16*, 1540–1548. [CrossRef]
120. Rosenfelder, R. Nuclear polarization shifts in light muonic atoms. *Nucl. Phys. A* **1983**, *393*, 301–313. [CrossRef]
121. Friar, J.L.; Payne, G.L. Higher-order nuclear-polarizability corrections in atomic hydrogen. *Phys. Rev. C* **1997**, *56*, 619–630. [CrossRef]
122. Pachucki, K.; Moro, A.M. Nuclear polarizability of helium isotopes in atomic transitions. *Phys. Rev. A* **2007**, *75*, 032521. [CrossRef]
123. Pachucki, K.; Patkóš, V.; Yerokhin, V.A. Three-photon-exchange nuclear structure correction in hydrogenic systems. *Phys. Rev. A* **2018**, *97*, 062511. [CrossRef]
124. Wauters, F.; Knecht, A. The muX project. *SciPost Phys. Proc.* **2021**, *5*, 022. [CrossRef]
125. Adamczak, A.; Antognini, A.; Berger, N.; Cocolios, T.E.; Deokar, N.; Düllmann, C.E.; Eggenberger, A.; Eichler, R.; Heines, M.; Hess, H.; et al. Muonic atom spectroscopy with microgram target material. *Eur. Phys. J. A* **2023**, *59*, 15. [CrossRef]
126. Rathi, S.; Valuev, I.A.; Sun, Z.; Heines, M.; Indelicato, P.; Ohayon, B.; Oreshkina, N.S. Theory Framework for Medium-Mass Muonic Atoms. *arXiv* **2026**, arXiv:2603.22021.
127. Li Muli, S.; Poggialini, A.; Bacca, S. Muonic Lithium atoms: Nuclear structure corrections to the Lamb shift. *SciPost Phys. Proc.* **2020**, *3*, 028. [CrossRef]
128. Gorchtein, M. A hitchhiker's guide to nuclear polarization in muonic atoms. *arXiv* **2025**, arXiv:2501.15274.
129. Valuev, I.A.; Colò, G.; Roca-Maza, X.; Keitel, C.H.; Oreshkina, N.S. Evidence Against Nuclear Polarization as Source of Fine-Structure Anomalies in Muonic Atoms. *Phys. Rev. Lett.* **2022**, *128*, 203001. [CrossRef]
130. Valuev, I.A.; Oreshkina, N.S. Full leading-order nuclear polarization in highly charged ions. *Phys. Rev. A* **2024**, *109*, 042811. [CrossRef]
131. Sun, Z.; Beyer, K.A.; Mandrykina, Z.A.; Valuev, I.A.; Keitel, C.H.; Oreshkina, N.S. ^{208}Pb Nuclear Charge Radius Revisited: Closing the Fine-Structure-Anomaly Gap. *Phys. Rev. Lett.* **2025**, *135*, 163002. [CrossRef]
132. Beyer, K.A.; Valuev, I.A.; Mandrykina, Z.A.; Sun, Z.; Oreshkina, N.S. Relativistic recoil as a key to the fine-structure puzzle in muonic ^{90}Zr. *arXiv* **2025**, arXiv:2511.22298.
133. Seng, C.Y. Radiative Corrections to Semileptonic Beta Decays: Progress and Challenges. *Particles* **2021**, *4*, 397–467. [CrossRef]

134. King, G.B.; Glick-Magid, A.; Sargsyan, G.; Caprio, M.A.; Leach, K.G.; Behr, J.A.; Bonaiti, F.; Brodeur, M.; Chambers-Wall, G.; Crawford, H.L.; et al. Future directions in nuclear β decay at FRIB and beyond. *arXiv* **2026**, arXiv:2607.22983.
135. Cabibbo, N. Unitary Symmetry and Leptonic Decays. *Phys. Rev. Lett.* **1963**, *10*, 531–533. [CrossRef]
136. Kobayashi, M.; Maskawa, T. CP-Violation in the Renormalizable Theory of Weak Interaction. *Prog. Theor. Phys.* **1973**, *49*, 652–657. [CrossRef]
137. Sirlin, A. Current algebra formulation of radiative corrections in gauge theories and the universality of the weak interactions. *Rev. Mod. Phys.* **1978**, *50*, 573–605. [CrossRef]
138. Fermi, E. Versuch einer Theorie der β-Strahlen. I. *Z. Für Phys.* **1934**, *88*, 161–177. [CrossRef]
139. Hill, R.J.; Plestid, R. All orders factorization and the Coulomb problem. *Phys. Rev. D* **2024**, *109*, 056006. [CrossRef]
140. Hill, R.J.; Plestid, R. Field Theory of the Fermi Function. *Phys. Rev. Lett.* **2024**, *133*, 021803. [CrossRef]
141. Sirlin, A. General Properties of the Electromagnetic Corrections to the Beta Decay of a Physical Nucleon. *Phys. Rev.* **1967**, *164*, 1767–1775. [CrossRef]
142. Sirlin, A.; Zucchini, R. Accurate Verification of the Conserved-Vector-Current and Standard-Model Predictions. *Phys. Rev. Lett.* **1986**, *57*, 1994–1997. [CrossRef]
143. Jaus, W.; Rasche, G. Radiative corrections to 0^+-0^+ β transitions. *Phys. Rev. D* **1987**, *35*, 3420–3422. [CrossRef]
144. Sirlin, A. Remarks concerning the $O(Z\alpha^2)$ corrections to Fermi decays, conserved-vector-current predictions, and universality. *Phys. Rev. D* **1987**, *35*, 3423–3427. [CrossRef]
145. Czarnecki, A.; Marciano, W.J.; Sirlin, A. Precision measurements and CKM unitarity. *Phys. Rev. D* **2004**, *70*, 093006. [CrossRef]
146. Vander Griend, P.; Cao, Z.; Hill, R.J.; Plestid, R. The Fermi function and the neutron's lifetime. *Phys. Lett. B* **2025**, *868*, 139678. [CrossRef]
147. Cao, Z.; Hill, R.J.; Plestid, R.; Vander Griend, P. The $Z\alpha^2$ correction to superallowed beta decays in effective field theory and implications for $|V_{ud}|$. *arXiv* **2025**, arXiv:2511.05446.
148. Seng, C.Y.; Gorchtein, M.; Ramsey-Musolf, M.J. Dispersive evaluation of the inner radiative correction in neutron and nuclear β decay. *Phys. Rev. D* **2019**, *100*, 013001. [CrossRef]
149. Seng, C.Y.; Feng, X.; Gorchtein, M.; Jin, L.C. Joint lattice QCD–dispersion theory analysis confirms the quark-mixing top-row unitarity deficit. *Phys. Rev. D* **2020**, *101*, 111301. [CrossRef]
150. Shiells, K.; Blunden, P.G.; Melnitchouk, W. Electroweak axial structure functions and improved extraction of the V_{ud} CKM matrix element. *Phys. Rev. D* **2021**, *104*, 033003. [CrossRef]
151. Czarnecki, A.; Marciano, W.J.; Sirlin, A. Radiative corrections to neutron and nuclear beta decays revisited. *Phys. Rev. D* **2019**, *100*, 073008. [CrossRef]
152. Satuła, W.; Dobaczewski, J.; Nazarewicz, W.; Rafalski, M. Microscopic Calculations of Isospin-Breaking Corrections to Superallowed Beta Decay. *Phys. Rev. Lett.* **2011**, *106*, 132502. [CrossRef]
153. Ormand, W.E.; Brown, B.A. Corrections to the Fermi Matrix Element for Superallowed β Decay. *Phys. Rev. Lett.* **1989**, *62*, 866–869. [CrossRef]
154. Navrátil, P.; Barrett, B.R. Large-basis shell-model calculations for *p*-shell nuclei. *Phys. Rev. C* **1998**, *57*, 3119–3128. [CrossRef]
155. Caurier, E.; Navrátil, P.; Ormand, W.; Vary, J. *Ab initio* shell model for A = 10 nuclei. *Phys. Rev. C* **2002**, *66*, 024314. [CrossRef]
156. Miller, G.A.; Schwenk, A. Isospin-symmetry-breaking corrections to superallowed Fermi β decay: Formalism and schematic models. *Phys. Rev. C* **2008**, *78*, 035501. [CrossRef]
157. Miller, G.A.; Schwenk, A. Isospin-symmetry-breaking corrections to superallowed Fermi β decay: Radial excitations. *Phys. Rev. C* **2009**, *80*, 064319. [CrossRef]
158. Auerbach, N.; Bui, M.L. Coulomb corrections to Fermi beta decay in nuclei. *Nucl. Phys. A* **2022**, *1027*, 122521. [CrossRef]
159. Belfatto, B.; Beradze, R.; Berezhiani, Z. The CKM unitarity problem: A trace of new physics at the TeV scale? *Eur. Phys. J. C* **2020**, *80*, 149. [CrossRef]
160. Cirigliano, V.; Crivellin, A.; Hoferichter, M.; Moulson, M. Scrutinizing CKM unitarity with a new measurement of the $K_{\mu3}/K_{\mu2}$ branching fraction. *Phys. Lett. B* **2023**, *838*, 137748. [CrossRef]
161. Seng, C.Y.; Gorchtein, M. Dispersive formalism for the nuclear structure correction $\delta_{\rm NS}$ to the β decay rate. *Phys. Rev. C* **2023**, *107*, 035503. [CrossRef]
162. US Department of Energy (USDOE). *A New Era of Discovery: The 2023 Long Range Plan for Nuclear Science*; Technical Report; Office of Science, US Department of Energy (USDOE): Washington, DC, USA, 2023. [CrossRef]
163. Sargsyan, G.H.; King, G.B.; Glick-Magid, A.; Seng, C.Y. The role of *ab initio* beta-decay calculations in light nuclei for probes of physics beyond the standard model. *Prog. Part. Nucl. Phys.* **2026**, *151*, 104260. [CrossRef]
164. King, G.B.; Carlson, J.; Flores, A.R.; Gandolfi, S.; Mereghetti, E.; Pastore, S.; Piarulli, M.; Wiringa, R.B. Quantum Monte Carlo calculation of $\delta_{\rm NS}$ in ^{10}C using an effective field theory approach. *Phys. Rev. C* **2026**, *114*, 015501. [CrossRef]
165. Cirigliano, V.; Dekens, W.; de Vries, J.; Gandolfi, S.; Hoferichter, M.; Mereghetti, E. Radiative Corrections to Superallowed β Decays in Effective Field Theory. *Phys. Rev. Lett.* **2024**, *133*, 211801. [CrossRef]

166. Cirigliano, V.; Dekens, W.; de Vries, J.; Gandolfi, S.; Hoferichter, M.; Mereghetti, E. *Ab initio* electroweak corrections to superallowed β decays and their impact on Vud. *Phys. Rev. C* **2024**, *110*, 055502. [CrossRef]
167. Plestid, R.; Wise, M.B. Vertex corrections and wavefunction renormalization for atoms, nuclei, and other heavy composite particles. *Phys. Rev. D* **2026**, *113*, 096011. [CrossRef]
168. Plestid, R.; Wise, M.B. Manifest Gauge Invariance for Structure Dependent Radiative Corrections to Processes Involving Atoms and Nuclei. *arXiv* **2025**, arXiv:2505.05449.
169. Seng, C.Y.; Gorchtein, M. Toward ab-initio nuclear theory calculations of δC. *Phys. Rev. C* **2024**, *109*, 044302. [CrossRef]
170. Piarulli, M.; Wiringa, R.B.; Lovato, A.; King, G.B.; Pastore, S. Quantum Monte Carlo calculation of δ_C in the superallowed beta decay of ^{10}C. *arXiv* **2026**, arXiv:2605.14006.
171. Donoghue, J.F.; Golowich, E.; Holstein, B.R. *Dynamics of the Standard Model*, 2nd ed.; Cambridge Monographs on Particle Physics, Nuclear Physics and Cosmology; Cambridge University Press: Cambridge, UK, 2014.
172. Kulagin, S.A.; Petti, R. Neutrino inclusive inelastic scattering off nuclei. *Phys. Rev. D* **2007**, *76*, 094023. [CrossRef]
173. Frankfurt, L.; Guzey, V.; Strikman, M. Leading twist nuclear shadowing phenomena in hard processes with nuclei. *Phys. Rep.* **2012**, *512*, 255–393. [CrossRef]
174. Kopeliovich, B.Z.; Morfín, J.G.; Schmidt, I. Nuclear shadowing in electro-weak interactions. *Prog. Part. Nucl. Phys.* **2013**, *68*, 314–372. [CrossRef]
175. Armesto, N. Nuclear shadowing. *J. Phys. G Nucl. Part. Phys.* **2006**, *32*, R367. [CrossRef]
176. Labelle, P. Effective field theories for QED bound states: Extending nonrelativistic QED to study retardation effects. *Phys. Rev. D* **1998**, *58*, 093013. [CrossRef]
177. Pineda, A.; Soto, J. Potential NRQED: The positronium case. *Phys. Rev. D* **1998**, *59*, 016005. [CrossRef]
178. Labelle, P.; Zebarjad, S.M. Derivation of the Lamb shift using an effective field theory. *Can. J. Phys.* **1999**, *77*, 267–278. [CrossRef]
179. Manohar, A.V.; Stewart, I.W. Logarithms of α in QED Bound States from the Renormalization Group. *Phys. Rev. Lett.* **2000**, *85*, 2248–2251. [CrossRef]
180. Fretwell, S.; Leach, K.G.; Bray, C.; Kim, G.B.; Dilling, J.; Lennarz, A.; Mougeot, X.; Ponce, F.; Ruiz, C.; Stackhouse, J.; et al. Direct Measurement of the ^{7}Be L/K Capture Ratio in Ta-Based Superconducting Tunnel Junctions. *Phys. Rev. Lett.* **2020**, *125*, 032701. [CrossRef]
181. Leach, K.G.; Friedrich, S. The BeEST Experiment: Searching for Beyond Standard Model Neutrinos Using ^{7}Be Decay in STJs. *J. Low Temp. Phys.* **2022**, *209*, 796–803. [CrossRef]
182. Carney, D.; Leach, K.G.; Moore, D.C. Searches for Massive Neutrinos with Mechanical Quantum Sensors. *PRX Quantum* **2023**, *4*, 010315. [CrossRef]
183. Li, G.; Segel, R.; Scielzo, N.D.; Bertone, P.F.; Buchinger, F.; Caldwell, S.; Chaudhuri, A.; Clark, J.A.; Crawford, J.E.; Deibel, C.M.; et al. Tensor Interaction Limit Derived From the $\alpha-\beta-\overline{\nu}$ Correlation in Trapped ^{8}Li Ions. *Phys. Rev. Lett.* **2013**, *110*, 092502. [CrossRef]
184. Sargsyan, G.H.; Launey, K.D.; Burkey, M.T.; Gallant, A.T.; Scielzo, N.D.; Savard, G.; Mercenne, A.; Dytrych, T.; Langr, D.; Varriano, L.; et al. Impact of Clustering on the ^{8}Li β Decay and Recoil Form Factors. *Phys. Rev. Lett.* **2022**, *128*, 202503. [CrossRef]
185. Nuber, J.; Adamczak, A.; Abdou Ahmed, M.; Affolter, L.; Amaro, F.D.; Amaro, P.; Antognini, A.; Carvalho, P.; Chang, Y.H.; Chen, T.L.; et al. Diffusion of muonic hydrogen in hydrogen gas and the measurement of the 1*s* hyperfine splitting of muonic hydrogen. *SciPost Phys. Core* **2023**, *6*, 057. [CrossRef]
186. Friar, J.L.; Payne, G.L. Nuclear corrections to hyperfine structure in light hydrogenic atoms. *Phys. Rev. C* **2005**, *72*, 014002. [CrossRef]
187. Ji, C.; Zhang, X.; Platter, L. Nuclear Structure Effects on Hyperfine Splittings in Ordinary and Muonic Deuterium. *Phys. Rev. Lett.* **2024**, *133*, 042502. [CrossRef]
188. Bonilla, J.; Richardson, T.R.; Bacca, S.; Ji, C.; Platter, L. Improved nuclear-structure corrections to the hyperfine splitting of electronic and muonic deuterium. *Phys. Lett. B* **2026**, *874*, 140257. [CrossRef]

Disclaimer/Publisher's Note: The statements, opinions and data contained in all publications are solely those of the individual author(s) and contributor(s) and not of MDPI and/or the editor(s). MDPI and/or the editor(s) disclaim responsibility for any injury to people or property resulting from any ideas, methods, instructions or products referred to in the content.